LITHOS 414-415 (2022) 106637

Contents lists available at ScienceDirect

LITHOS

journal homepage: www.elsevier.com/locate/lithos

Mid-Cretaceous intra-oceanic arc-continent collision recorded by the igneous complex in central Myanmar

Zong-Yong Yang [a], Xian-Wu Bi [a,b], Jing-Jing Zhu [a,*], Ruizhong Hu [a,b], Hong Zhong [a,b], Kyaing Sein [c], Than Zaw [c], Dian-Zhong Wang [a]

[a] State Key Laboratory of Ore Deposit Geochemistry, Institute of Geochemistry, Chinese Academy of Sciences, Guiyang 550081, China
[b] College of Earth and Planetary, University of Chinese Academy of Sciences, Beijing 100049, China
[c] Myanmar Geosciences Society, Yangon, Myanmar

ARTICLE INFO

Keywords:
Intra-oceanic arc
Neo-Tethys Ocean
Collision event
Cretaceous
Myanmar

ABSTRACT

Magmatic rocks from intra-oceanic arcs are critical for understanding the formation of continental crust and tectonic evolution. The early tectonic evolution of the Neo-Tethyan Ocean before the final Indo-Asia collision remains mysterious, and the geodynamic processes that triggered the Cretaceous magmatism in central Myanmar is still debated. The Cretaceous magmatic complex in the Banmauk-Kawlin area (BKC), west Myanmar terrane (WMT) is composed of the Kanza Chaung granitoid batholith, the Mawgyi Volcanic rocks, and the Pinhinga plutonic complex. Zircon U-Pb dating results of various rocks from the Kanza Chaung batholith suggest magmatism lasted from ca. 110 to ca. 94 Ma, roughly overlapping with new geochronological data for the Mawgyi Volcanics. Mafic rocks, including basalts from the Mawgyi Volcanics and gabbros from the Kanza Chaung Batholith, have geochemical features resembling intra-oceanic arc magmas, characterized by high large-ion-lithophile elements (LILEs) and low high-field-strength elements (HFSEs) and flat trace element patterns. They have depleted Sr (initial $^{87}Sr/^{86}Sr = 0.7035–0.7054$) and Nd ($\varepsilon Nd(t) = 0.39–6.71$) isotopic compositions, with zircon $\varepsilon Hf(t)$ values ranging from +5.8 to +16.1, probably derived from partial melting of the mantle wedge. Diorites formed by differentiation of basaltic magma have similar trace element patterns and Sr-Nd isotopes. The granitic rocks were likely originated from partial melting of juvenile arc lower-crust, indicated by their high SiO_2 (>65.0 wt%), low MgO (<2.50 wt%) and depleted Nd and zircon Hf isotopes. The $\varepsilon Nd(t)$ values of the BKC shift markedly (from ~ + 7 to 0) from 105 to 94 Ma, which correlates with a temporal increase of Th/Nb, La/Ta, and La/Sm. Given the juvenile characteristics of the WMT crust, this can be explained by exotic isotopically enriched crustal components subducted into the mantle source, rather than steady-state sediment subduction and crustal contamination. Given the Albian unconformity in the WMT and recent paleomagnetic data, such continent crustal components were likely introduced by collision followed by subduction of Greater India-derived continental sliver beneath the WMT. Thus crust with an Indian continent affinity was possibly accreted to an intra-oceanic arc (WMT) during the mid-Cretaceous.

1. Introduction

Closure of the Neo-Tethys Ocean between the Asian and Indian continental lithosphere has been commonly ascribed to continuous oceanic slab subduction (Yin and Harrison, 2000; Zhang et al., 2018), based on magmatic and detrital zircon records (Chu et al., 2011; Wu et al., 2010; Zhang et al., 2019). The Neo-Tethys slab subduction beneath the Asian continent was likely initiated during the Triassic (Ma et al., 2013; Wang et al., 2019a), and involved at least two intra-oceanic arcs including the Kohistan and the West Myanmar terranes (WMT; Clift et al., 2002; Jagoutz et al., 2015; Westerweel et al., 2019). However, it remains ambiguous how and when the subduction of Neo-Tethys oceanic lithosphere was interrupted by welding of continental crust slivers with intra-oceanic arcs before the final India-Asia collision (e.g., Jagoutz et al., 2015; Martin et al., 2020; Morley et al., 2020). Cretaceous magmatic rocks in central Myanmar are closely related to the Neo-Tethyan evolution and have been considered to be related either to Andean-type continental arcs formed by the prolonged subduction of the

* Corresponding author.
E-mail address: zhujingjing@vip.gyig.ac.cn (J.-J. Zhu).

https://doi.org/10.1016/j.lithos.2022.106637
Received 1 September 2021; Received in revised form 11 February 2022; Accepted 15 February 2022
Available online 18 February 2022

Neo-Tethyan oceanic slab (Zhang et al., 2018) or to intra-oceanic arcs (Westerweel et al., 2019) formed by forced subduction initiation (Zhang et al., 2021b). Resolving this is crucial for improving our understanding of the geodynamics of Neo-Tethys Ocean subduction, the evolution of the convergence of India with Eurasia (Jagoutz et al., 2015; Morley et al., 2020; van Hinsbergen., 2019; Westerweel et al., 2019), and the geometry of the Greater India. Here we suggest that Greater India is a hyperextended continental fragment from the northern margin of India, based on paleomagnetic data and crustal shortening estimates from Tibet (e.g., Martin et al., 2020; van Hinsbergen et al., 2012).

The Gangdese arc, exposed on the southern margin of the Asian continent, is a typical and direct product of the consumption of the Neo-Tethyan ocean crust (Wu et al., 2010; Yin and Harrison, 2000). It is dominantly composed of Late Cretaceous and Paleogene granitoids, with subordinate Early Cretaceous to Triassic magmatic rocks (Ma et al., 2013; Wang et al., 2019a and references therein). The relative lack of mid-Cretaceous magmatism could be a consequence of erosion caused by later uplift (Ji et al., 2014; Wu et al., 2010). Hence, this outcrop pattern implies loss of material related to underthrusting of the Neo-Tethys oceanic crust before the Late Cretaceous.

Magmatic rocks exposed along the spine of the WMT consist mainly of the Wuntho-Popa arc (WPA, Fig. 1a). Previous geochronological data support long-lived magmatic activity that began in the Early Cretaceous given the ca. 107 Ma zircon ages of magmatic rocks from both the Mawgyi Volcanic rocks and the Kanza Chaung batholith (Li et al., 2020; Licht et al., 2020; Zhang et al., 2021b), and lasted to the Late Cenozoic, culminating in the mid-Cretaceous (Lee et al., 2016; Licht et al., 2020; Mitchell et al., 2012; Zhang et al., 2021b). It bridges the Himalayan-Tibet orogeny belt around the eastern Himalayan syntaxis to the north and the Andaman-Sunda subduction zone to the south (Li et al., 2020). The similarity in magmatic history and isotopic compositions between the WPA and the Gangdese arc of the Lhasa Terrane (Li et al., 2020; Lin et al., 2019; Zhang et al., 2018) suggest that the WPA is a continuation of the Gangdese arc, but their distinct zircon U-Pb age spectrum argues against this (Licht et al., 2020). Recent paleomagnetic data suggest that the mid-Cretaceous western Myanmar terrane was located at a near equator latitude in an intra-oceanic arc setting (Jagoutz et al., 2015; Licht et al., 2020; Westerweel et al., 2019). Consequently, more work is necessary to carefully evaluate the generation of Cretaceous magmatism in central Myanmar, which would improve our understanding of the early geodynamic evolution of the Neo-Tethys Ocean.

In the present study, geochronological, and geochemical data for igneous rocks from the main body of the WPA, exposed west of Banmauk and Kawlin in Myanmar, are reported. These datasets combined with previous published data provide clues to an intra-oceanic arc-continent collision event before the early Cenozoic India-Asia collision.

2. Geological setting and samples

2.1. Tectonic framework

Myanmar, from east to west, comprises the Sibumasu terrane, WMT, and Indo-Burma Range (IBR), separated by Myitkyina and Kalaymyo (ultra-) mafic igneous belts (Fig. 1a). The Sibumasu terrane (Metcalfe, 2013) is located in eastern Myanmar, separated from the WMT by the dextral strike-slip Sagaing Fault, as indicated by the contrasting magmatic associations and degrees of metamorphism across this boundary (Barber et al., 2017; Gardiner et al., 2018; Searle et al., 2007). The Sibumasu terrane is interpreted to have originated from the Gondwana super continent and collided with eastern Indochina terrane during the Triassic (Metcalfe, 2013), and is characterized by widespread Precambrian to Late Mesozoic carbonate and clastic rocks. On the western margin of the Sibumasu terrane lies the Mogok Metamphic Belt (MMB), composed of metamorphosed sedimentary rocks, numerous granites and meta-granites (Barley et al., 2003; Khin Zaw, 1990). In the Mandalay region of the MMB, marbles with calc-schist laminations

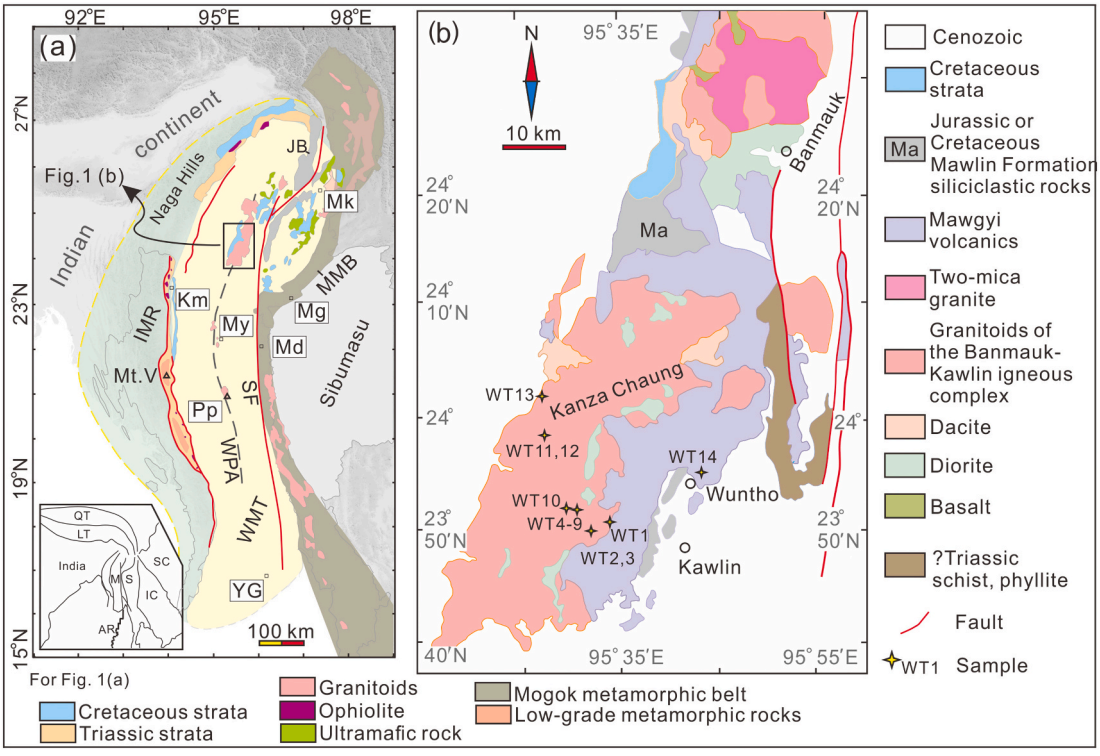

Fig. 1. Simplified geological map of Myanmar showing (a) the major tectonic units of Myanmar, modified from Cai et al. (2019) and (b) igneous complexes in the Banmauk-Kawlin area (BKC), modified after Mitchell (2018) and Zhang et al. (2018).
IBR: Indo-Burma Range; JB: Jade belt; MMB: Mandalay-Mogok metamorphic belt; SF: Sagaing Fault; WMT: West Myanmar terrane; City or county: Km = Kalaymyo; Md = Mandalay; Mg = Mogok; Mk = Myitkyina; My = Monywa; Mt.·V = Mt. Victoria Land; Pp = Mt. Popa; YG = Yangon.

resemble fossiliferous Ordovician to Early Devonian carbonates of the interior Sibumasu (Mitchell et al., 2007).

The Myitkyina mafic rock suites have been interpreted to be either relict oceanic lithosphere derived from the Meso-Tethys Ocean (Liu et al., 2016) or a Jurassic magmatic arc based on enrichments in large ion lithophile elements (LILEs) and depletions in high field strength elements (HFSEs, Zhang et al., 2018).

The WMT is divided by the WPA into the Eastern and Western Troughs (Mitchell, 1993). The Western Trough is characterized by Upper Cretaceous–Quaternary sedimentary rocks, and interpreted to be a fore-arc basin (Barber et al., 2017; Cai et al., 2019; Yao et al., 2017). The Eastern Trough consists of Paleo- and Neogene non-marine sediments (Htut, 2017). The WPA consists of discontinuous exposures of Cretaceous tholeiitic to calc-alkaline magmatic rocks and the Mawgyi Volcanic rocks. Recent zircon U-Pb and whole-rock $^{40}Ar/^{39}Ar$ isotopic results for the Mawgyi Volcanics indicate magmatism lasted from ca. 106 to 94 Ma (Westerweel et al., 2019; Zhang et al., 2021b). The magmatism associated with the Banmauk-Kawlin igneous complex (BKC; Fig. 1b) initiated at ca. 110 Ma and ceased at ca. 90 Ma (Li et al., 2020; Licht et al., 2020; Lin et al., 2019), broadly overlapping the adjacent Mawgyi Volcanic rocks. Field observations show that the Mawgyi Volcanics are intruded by the granitic rocks of Kanza Chaung batholith (Mitchell, 1993; United Nations, 1978), but geochronological studies show that they are broadly coeval (Gardiner et al., 2017; Licht et al., 2020; Lin et al., 2019; Zhang et al., 2021b). Furthermore, the absence of pre-130 Ma zircon in sediments from rivers draining the Mawgyi Volcanics suggests they were emplaced no earlier than the Early Cretaceous (Licht et al., 2020). Taken together, this suggests that the Mawgyi volcanics formed in the mid-Cretaceous and are slightly older than the granitic rocks. This magmatic belt has been suggested to be a west-facing arc closely related to Neo-Tethys ocean subduction (Lin et al., 2019; Mitchell and McKerrow, 1975; Zhang et al., 2018).

Near the Indo-Myanmar border, the IBR and dismembered ultramafic blocks (metamorphic zircon age of ca. 115 Ma) have been considered to be an accretionary wedge and ophiolites related to Neo-Tethys slab subduction (Liu et al., 2016; Mitchell and McKerrow, 1975). In the Mt. Victoria Land region (Fig. 1a), the IBR consists of Cretaceous ophiolites, Triassic turbidites of the Pane Chaung Formation, and underlying Kanpetlet mica schist, which are in turn overlain unconformably by Upper Albian to Cenomanian limestones (ca. 110–90 Ma; Mitchell, 1993; Morley et al., 2020).

2.2. Metamorphic rocks in Myanmar

Metamorphic rocks in Myanmar occur mainly in the Banmauk, Jade Mines Belt, Myitkyina, Katha and the Mogok areas. Metamorphic rocks around Banmauk consist of gneiss, mica schist, and amphibolite (Mitchell, 2018). The timing of metamorphism and their protolith have not been well constrained. Detrital zircons from sands in rivers draining the metamorphic rocks around Banmauk area show no Precambrian grains and have consistent ages of ca. 110–90 Ma (Licht et al., 2020).

It has been suggested that the metamorphic rocks in Banmauk were similar to those in the Jade Mines Belt, Myitkyina, Katha and the Mogok areas (Mitchell, 2018). All of them are bounded by faults that splay off the northern termination of the Sagaing Fault, and thus their correlation is ambiguous (Searle et al., 2017). Isotopic dating suggests that the metamorphic rocks in the Jade Mines Belt are post-Triassic (Searle et al., 2017; Yui et al., 2013). Gneiss exposed in the north of the Myigkyina area has yielded Paleogene zircon U-Pb ages (Lin et al., 2019). Eclogite boulders from the Kumon range suggest high-pressure metamorphism, but no ages have been reported (Enami et al., 2012). Quartzites and mica schist with local kyanite in Katha, east of the Sagaing Fault, have age peaks at ca. 500 Ma and 850–1200 Ma (Zhang et al., 2018).

2.3. Mesozoic–Cenozoic magmatism in WMT

The magmatic complex exposed in the Banmauk and Kawlin region (BKC) forms the northern part of the WPA, consisting largely of granodiorite, with minor diorite, granite and gabbro sills and/or dikes (Fig. 1b). They have mid-Cretaceous emplacement ages (Gardiner et al., 2017; Li et al., 2020; Mitchell et al., 2012; Zhang et al., 2017). Two-mica granites from the Pinhinga plutonic complex (United Nations, 1978) north of Banmauk were also emplaced in the mid-Cretaceous (ca. 100 Ma; Lin et al., 2019).

The MMB, the westernmost part of the Sibumasu terrane, contains Late Mesozoic to Cenozoic igneous rocks. Jurassic magmatic rocks have been reported from the Myitkyina region (Clegg, 1941; Gardiner et al., 2018; Khin Zaw, 1990; Liu et al., 2016), of which the ca. 172 Ma diorites have geochemical compositions similar to oceanic plagiogranites (Liu et al., 2016). Mesozoic magmatic rocks in the MMB are mainly Cretaceous granitoids (Barley et al., 2003; Gardiner et al., 2018; Mitchell et al., 2012), suggesting a period of crustal re-melting (Gardiner et al., 2018 and reference therein; Lin et al., 2019). Cenozoic magmatic rocks are mainly exposed along the WPA, such as in the southernmost end of the BKC, the volcanic rocks in Monywa, and basalt, andesite in Mt. Popa (Lee et al., 2016; Li et al., 2019a; Lin et al., 2019).

2.4. Petrography of the Banmauk-Kawlin igneous complex

The BKC includes granitic to quartz dioritic rocks and locally gabbro, but granodiorite is the predominant rock phase (Fig. S1a, b; Mitchell, 2018). Lower Cretaceous or Jurassic volcanic rocks (i.e., the Mawgyi Volcanics) are composed of basalt with andesite–dacite dikes (Mitchell, 1993; Zhang et al., 2021b). They were intruded by tonalitic and granodioritic plutons of the BKC (Mitchell, 1993; United Nations, 1978). Mawgyi Volcanics, northeast of Wuntho city, are porphyritic with phenocrysts (~35 vol%) of plagioclase and clinopyroxene in a fine-grained matrix.

Petrographic characteristics of intrusive rocks for the Kanza Chaung batholith (Fig. S1) have been described by Li et al. (2020) and are only described briefly here. Gabbros are medium- to fine-grained (Fig. S1c), consisting mainly of plagioclase, amphibole, and clinopyroxene. Two groups of amphibole have been identified (Fig. S1c). Type I is green or brownish-green, showing no diagnostic cleavages but with irregular grain boundaries and generally containing clinopyroxene relicts; type II amphibole is brown, showing well-defined planar grain boundaries and oblique cleavage planes at around 56 degrees. Type I amphibole could be formed by replacement due to metasomatic reactions during the later stage of magma evolution (e.g., Coogan et al., 2001). The second type of amphibole is of magmatic origin. Diorites have less clinopyroxene relative to the gabbros, mafic mineral phases consist of amphibole and biotite, and quartz occurs as an interstitial phase. Felsic intrusive rocks include granodiorite (Fig. S1d) and less granitic dikes or stocks (Fig. S1e).

3. Analytical methods

3.1. Zircon U-Pb and Hf isotopes

Whole-rock major, trace and rare earth elements (REE) as well as Sr-Nd isotopic compositions were measured for 13 representative samples, including one from the Mawgyi Volcanic rocks (WT14) with the remainder from the Kanza Chaung batholith. Ten samples were dated by zircon U-Pb analyses, and zircon Lu-Hf isotopes were completed on 6 samples after U-Pb isotope analysis.

Zircon grains were separated using conventional density and magnetic methods. The zircon crystals were mounted in epoxy and polished to expose their internal section. Transmitted and reflected photomicrographs were imaged with an optical microscope, cathodoluminescent (CL) images were taken with a JXA8530F-plus electron microprobe,

housed at the State Key Laboratory of Ore Deposit Geochemistry, Institute of Geochemistry, Chinese Academy of Sciences (SKLODG, IGCAS), for elemental zoning and texture examination. Optional spot positions for in situ U-Pb and Lu-Hf isotopic analyses were selected from these images. The U-Pb analyses were conducted on a 7500a quadruple (Q)-ICP-MS equipped with a 193 nm excimer ArF laser-ablation system. Off-line data calculation was conducted on ICPMS DataCal (Liu et al., 2008). Age uncertainties for a single spot are cited at the 1σ level and the weighted mean ages are quoted at the 95% confidence level.

During the course of analysis, the unknown Qinghu zircon yielded a weighted mean age of 158.7 ± 1.8 Ma (n = 9). The Plešovice zircon yielded a mean age of 337.2 ± 2.7 Ma (n = 13). The standard zircon 91,500 given an age of 1062.4 ± 5.8 Ma (n = 31). These results are consistent with the suggested values within uncertainty (Li et al., 2013; Sláma et al., 2008; Wiedenbeck et al., 1995).

Zircon Lu-Hf isotopic compositions were carried out on a Nu Plasma III Multi-collector ICP-MS equipped with a Geolas 193 nm Resonetics RESOlution S-155 laser-ablation system, at the SKLODG, IGCAS. Instrumental run conditions and data acquisition are detailed by Hu et al. (2012). The same sites or the same zircon growth zones close to the U-Pb isotope analysis spots were targeted for Hf isotope analyses. A laser beam size of 60 μm was used. During the analytical procedure, standard zircon 91,500 yielded $^{176}Hf/^{177}Hf$ ratios of 0.282306 ± 0.000022, the unknown zircon Mud Tank, and Penglai gave $^{176}Hf/^{177}Hf$ ratios of 0.282516 ± 0.000014 and 0.282909 ± 0.000022, respectively. All are within the uncertainties of recommended values for these references (Li et al., 2010; Woodhead and Hergt, 2010).

3.2. Whole-rock geochemical compositions

Rock samples were cut into small chips and the fresh interior parts were cleaned with water, then dried before being crushed to 200 mesh powder. A steel mortar was used for rock crushing and sequential ground. Major elements were measured using an X-ray fluorescence spectrometer (XRF), at the ALS Laboratory Group, Guangzhou, China. Analytical precision is better than 2%. Trace and rare earth elements (REE) were determined by inductively coupled plasma mass spectrometry (ICP-MS) at the SKLODG, IGCAS. The analytical accuracy and precision are better than 5%. Analytical procedures are detailed by Qi et al. (2000).

Bulk-rock Sr-Nd isotope analyses were performed on a Neptune Plus MC-ICP-MS at the Nanjing FocuMS Technology Co. Ltd., China. Rock powders (~50 mg) were digested and dissolved with distilled HF-HNO_3 in high-pressure Teflon bombs for 3 days at 195 °C. Strontium and rare earth element (REE) were separated using cation exchange columns, and Nd was separated and purified from the other REEs on a column using HDEHP-coated Teflon powder as the ion exchange medium. The measured $^{87}Sr/^{86}Sr$ and $^{143}Nd/^{144}Nd$ ratio were normalized to $^{86}Sr/^{88}Sr$ = 0.1194 and $^{146}Nd/^{144}Nd$ = 0.7219, respectively. During the analytical procedure, the USGS standard references AGV-2, BCR-1, and BHVO-2 yielded $^{87}Sr/^{86}Sr$ ratios of 0.703990, 0.705026, and 0.703505; and $^{143}Nd/^{144}Nd$ ratios of 0.512779, 0.512628, and 0.512986, respectively. These are consistent with recommended values within uncertainty (Weis et al., 2006).

4. Results

4.1. Zircon feature and U-Pb isotopic reuslts

The zircon U-Pb dating results (Appendix Table 1) and representative CL images are detailed in Fig. 2 and Fig. S2. Zircons from gabbroic rocks and diorites are generally euhedral to subhedral, most of them display broad zoning in CL images. They have variable U (97.8 to 453.9 ppm) and Th/U mostly higher than 0.40. Most zircon crystals from granitic rocks are euhedral and concentric oscillatory zoning is common. Well-developed zircon zoning and high Th/U ratios indicate these zircons are of magmatic origin (Hoskin and Schaltegger, 2003).

A total of four gabbro samples were dated. Sample WT3 yielded $^{206}Pb/^{238}U$ apparent ages ranging from 54.2 to 110.2 Ma. Analyses with age significantly deviated from the majority of age population and show low concordance have been omitted as they likely result from Pb loss. After excluding these outliers, 19 analyses provided a lower intercept age of 97.9 ± 1.1 Ma, and a weighted mean age of 97.9 ± 1.0 Ma (MSWD = 0.55, n = 19; Fig. 2a). Zircons collected from sample WT7 yielded a mean age of 97.8 ± 1.1 Ma (MSWD = 0.39, n = 6; Fig. S2a). Sample WT8 had a lower intercept age of 97.1 ± 3.4 Ma and a weighted mean age of 98.6 ± 1.5 Ma (MSWD = 1.3, n = 11; Fig. S2b). Nineteen analyses were carried out on sample WT9, yielding intercepts at 97.8 ± 1.2 Ma on the Tera-Wasserburg plot line and yielded a weighted mean age of 97.8 ± 1.0 Ma (MSWD = 0.05; Fig. S2c).

Twenty-two analyses were carried out on the basaltic dike WT12, yielding $^{206}Pb/^{238}U$ apparent ages ranging from 90.0 ± 1.5 Ma to 110.1 ± 1.5 Ma. One crystal yielded a $^{206}Pb/^{238}U$ age of 110.1 ± 1.5 Ma, indicative of an antecryst. The remaining spots plot on or near the converse curve, and they intercept at 96.7 ± 1.2 Ma and provide a weighted mean age of 96.5 ± 1.3 Ma (MSWD = 1.2, n = 21; Fig. S2d).

Twenty-five zircon crystals were analyzed from diorite WT13. They have $^{206}Pb/^{238}U$ apparent ages ranging from 97.2 ± 2.0 Ma to 106.3 ± 1.9 Ma. The analyzed zircon grains yielded a weighted mean age of 99.2 ± 1.2 Ma (MSWD = 1.1, n = 25) and a lower intercept age of 104 ± 4.2 Ma (Fig. 2b).

Twenty-five zircon grains from granodiorite sample WT10 were analyzed. One analysis yielded an apparent $^{206}Pb/^{238}U$ age of 136.4 ± 3.6 Ma, indicative of an antecrystic zircon. The remaining twenty-four spots yielded a lower intercept age of 95.8 ± 1.4 Ma and a weighted mean age of 95.9 ± 1.1 Ma (MSWD = 0.44, n = 24; Fig. S2e). Zircons from another granodiorite sample, WT11, yielded a lower $^{206}Pb/^{238}U$ intercept age of 97.4 ± 0.98 Ma and a weighted mean age of 96.7 ± 0.77 Ma (MSWD = 0.87, n = 23; Fig. 2c).

Zircons for granite sample WT6 yielded $^{206}Pb/^{238}U$ apparent age from 66.3 to 104.2 Ma and yielded a weighted mean age of 100 ± 3.0 Ma (MSWD = 1.9, n = 6; Fig. S2f). Thirteen spots of granitic dike sample WT2 plot on or near the Concordia line, they yielded a weighted mean age of 110.5 ± 1.5 Ma (MSWD = 0.96) and intercept at 110.5 ± 1.5 Ma (Fig. 2d). One analysis provided a $^{206}Pb/^{238}U$ age of 120.2 ± 2.0 Ma, possibly representing a captured crystal from the early phase of the Mawgyi Volcanics.

4.2. Major and trace elements

The BKC contains sub-alkaline rock types ranging from gabbro to granite with SiO_2 varying from 42 to 79 wt% (Appendix Table 2; Fig. 3a, b). Most of them belong to the tholeiitic to middle-K_2O calc-alkaline series (Fig. 3c, d).

Gabbros from the BKC have MgO contents ranging from 4.30 to 7.21 wt% (Fig. S3) and Mg# (molar Mg/(Mg + Fe) of 41 to 65. Two diorite samples have low MgO of 3.18 and 3.42 wt%. The two granodiorites and four granitic rock samples have high SiO_2 contents (66.2–78.9 wt%), low $Fe_2O_3^t$ (2.13–4.17 wt%) and MgO (0.47–1.17 wt%). The rock series from mafic through intermediate to felsic rocks defined broadly continuous linear trends (Fig. S3). With increasing silica, their MgO, FeO^t, CaO, and TiO_2 contents decrease, whereas the P_2O_5 contents decrease at SiO_2 > 60 wt%.

Most gabbro samples display coherent chondrite-normalized REE patterns (Fig. 4a) with slight enrichment of light REE (LREE, La/Yb_N = 1.3–3.1, the subscript N denotes chondrite normalization), and variable Eu anomalies (Eu/Eu* = 0.98–1.35). The exception is sample WT12, which has higher total REE contents than the rest of the gabbros, showing a convex upward LREE pattern and moderate Eu negative anomaly (Eu/Eu* = 0.59). One volcanic rock (WT14) has higher LREE contents (La/Yb_N = 8.7). Diorite, granodiorite and granite samples show mildly to strongly fractionated REE patterns (Fig. 4a, c), and they have

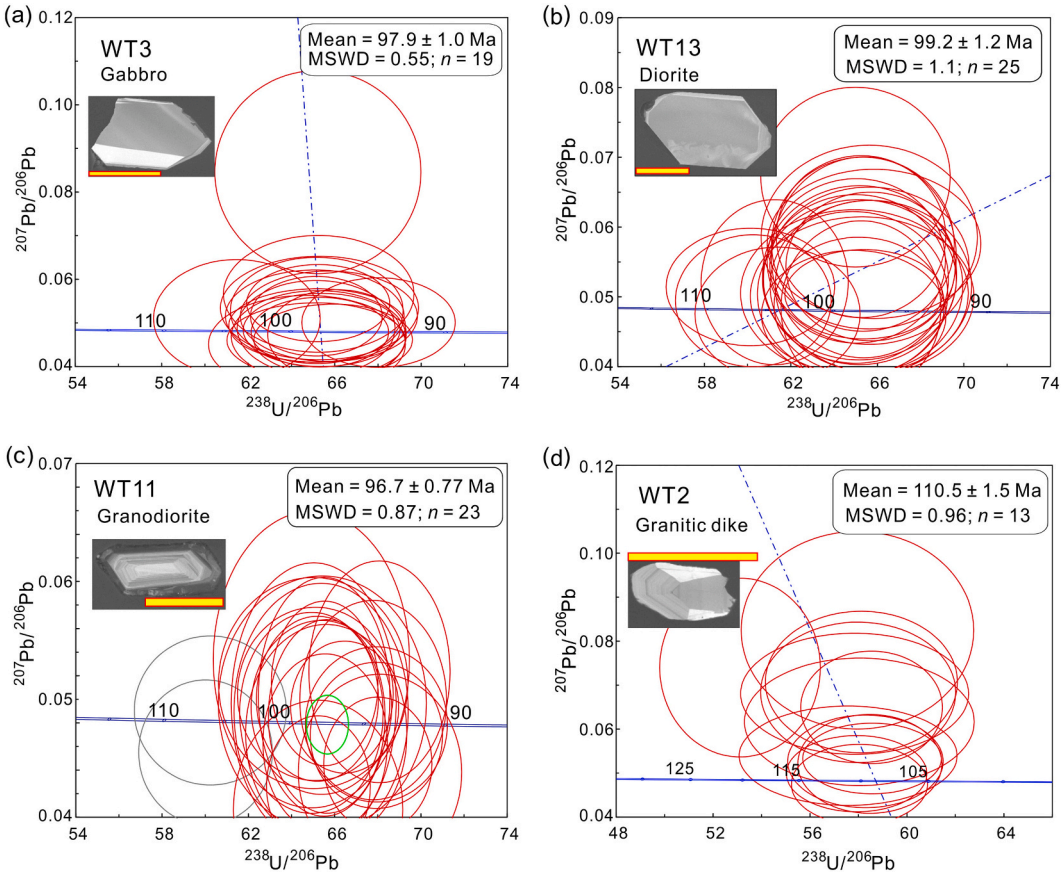

Fig. 2. Representative zircon U-Pb dating results and CL images.

$(La/Yb)_N$ ratios ranging from 1.5 to 5.7.

All of the gabbro and diorite rocks have arc-like trace elements patterns on primitive mantle normalized spider diagrams (Fig. 4b), characterized by enriched LILEs (e.g., Ba, Th) and depleted HFSEs (e.g., Nb, Ta, Ti). The granodiorite and granite rocks also have high LILE contents and low HFSEs, typical of arc derived igneous rocks (Fig. 4d).

4.3. Bulk-rock Sr-Nd isotopes

The various rock types from the BKC all show radiogenic Nd isotopes (Appendix Table 3; Fig. 5), with initial $^{143}Nd/^{144}Nd$ ratios (calculated at 110 Ma for WT1 and WT2 and 98 Ma for the others) ranging from 0.512616 to 0.512963 and $\varepsilon_{Nd}(t)$ values between +0.39 and + 6.71. These samples have $^{87}Sr/^{86}Sr$ of 0.7048–0.7055, with corresponding initial $^{87}Sr/^{86}Sr$ ratios of 0.7035–0.7054.

4.4. Zircon Hf isotopes

All analyzed zircons yielded high Hf isotopic composition with $\varepsilon_{Hf}(t)$ values >5 (Appendix Table 4; Fig. 6). For the three gabbro samples, analyzed crystals have $^{176}Hf/^{177}Hf$ ratios ranging from 0.2829925 to 0.2831703 and positive ε_{Hf} ($t = 98$ Ma) values between +9.8 and + 16.1. Sample WT8 has $\varepsilon_{Hf}(t)$ values ranging from +10.3 to +12.5, similar to those of the sample WT9 (from +8.7 to +11.8). These mafic rocks yielded young depleted mantle model ages (T_{DM}) ranging from 424 to 119 Ma.

The diorite sample WT13 yielded slightly more evolved zircon Hf isotopic compositions with $\varepsilon_{Hf}(t)$ values which range ranging from +7.2 to +9.5 and T_{DM} varying from 475 to 379 Ma. Ten analyses for sample WT12 yielded $\varepsilon_{Hf}(t)$ values ranging from +6.7 to +11.4 and T_{DM} from 530 to 305 Ma.

Granodiorite samples WT10 and WT11 have broadly similar $\varepsilon_{Hf}(t)$ values, from +8.2 to +12.2 and + 6.0 to +11.2, respectively. These analyzed zircon crystals have similar depleted mantle model ages from 532 to 251 Ma.

5. Discussion

5.1. Crustal nature of the West Myanmar Terrane

A ~ 20 m.y. period of mid-Cretaceous magmatism has been corroborated by zircon U-Pb dating for various rock types from the BKC. One gabbro sample yielded a mean age of 106.7 ± 0.6 Ma (Li et al., 2020). In the present study, a granitic dike provided a weighted mean age of 110.5 ± 1.5 Ma (Fig. 2d). The diorites dated by Li et al. (2020) yielded ages of 89.8 ± 0.7 and 90.6 ± 0.6 Ma, which are representatives of the latest magma of the BKC. Recent zircon U-Pb and whole-rock $^{40}Ar/^{39}Ar$ isotopic results for the Mawgyi Volcanic rocks indicate magmatism last from ca. 106 to 94 Ma (Westerweel et al., 2019; Zhang et al., 2021b). The magma pulse of the BKC initiated at ca. 110 Ma and ceased at ca. 90 Ma (This study; Gardiner et al., 2017; Li et al., 2020; Licht et al., 2020; Mitchell et al., 2012), partly overlapping the adjacent Mawgyi Volcanic rocks.

No ancient Precambrian magmatic rock has been identified in the WMT, and thus it is generally accepted to be comprised of juvenile crust (Gardiner et al., 2018; Licht et al., 2020; Lin et al., 2019). In the present study, the zircon from felsic rocks showing no Precambrian inherited core also implies an absence of ancient rocks underneath the WMT (Appendix Table A1). As mentioned previously, Precambrian metamorphic rock has not yet been verified from the WMT, even in the MMB (e.g., Lin et al., 2019; Searle et al., 2017; Yui et al., 2013). Sands from eleven rivers draining metamorphic rocks exposed around Banmauk

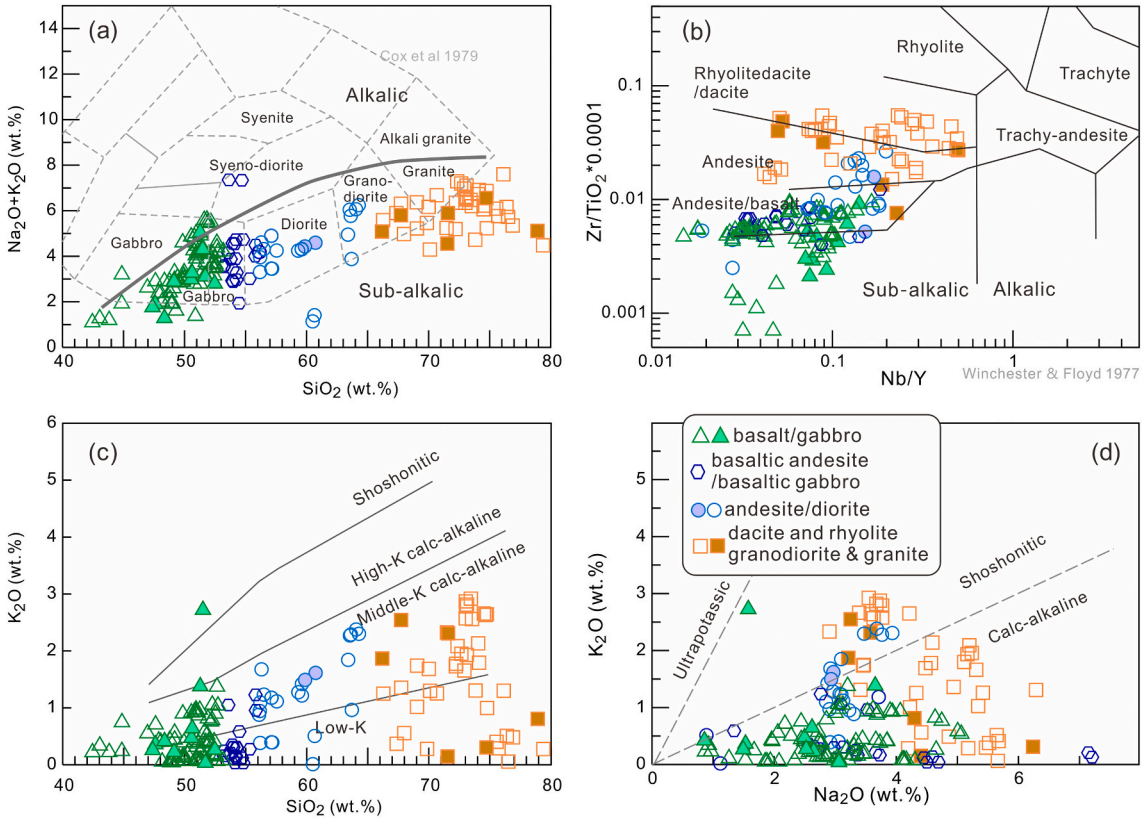

Fig. 3. Plot of total alkali-silica (TAS, a) for Cretaceous rocks from the BKC, Myanmar. Geochemical discrimination diagram for magmatic rocks (b; after Winchester and Floyd, 1977). Plots of K_2O vs SiO_2 (c; Peccerillo and Taylor, 1976) and N_2O contents (d). Open symbols refer data from (Li et al., 2020; Licht et al., 2020; Zhang et al., 2021b), the legend same in the following figures unless otherwise specified.

area yielded detrital zircon U-Pb ages of ca. 100 Ma, without Precambrian grain (Licht et al., 2020). Sedimentary rocks in the WMT are predominantly of Cretaceous to Cenozoic age (Cai et al., 2019; Zhang et al., 2017). Zircons extracted from both magmatic and siliciclastic sediments in the WMT are characterized mostly by depleted Hf isotopic compositions (Fig. 6; Gardiner et al., 2018; Li et al., 2020; Lin et al., 2019; Wang et al., 2014b). This is consistent with the magmatic rocks from WMT, which have depleted Nd isotope and young two stage depleted mantle model age (870–360 Ma; Appendix Table 3; Li et al., 2020; Mitchell et al., 2012; and see review of Zhang et al., 2018).

In contrast, Early Ordovician schists and gneisses have been found in the Naga Hills area within the IBR, to the west of WMT (Aitchison et al., 2019). In addition, Triassic Pane Chaung Formation and underlying metamorphic rocks crop out further south along the IBR, west of the ophiolite in the IBR. They contain Precambrian detrital zircons, showing an affinity with Greater India like the Langjiexue Group in the Tethyan Himalaya (Yao et al., 2017). Cretaceous to Eocene sedimentary rocks in the Chindwin basin have zircon grains with ages <200 Ma (Wang et al., 2014b).

Newly obtained paleomagnetic data from the Kanza Chaung batholith and Mawgyi Volcanic rocks suggests that the WMT was situated at S4.7 ± 5° from ca. 100–95 Ma (Westerweel et al., 2019). This would place it thousands of kilometers from the southern Asia margin and suggests that the WMT was part of the Trans-Tethyan intra-oceanic arc (Licht et al., 2020; Westerweel et al., 2019; Zhang et al., 2021b). The intra-oceanic arc model for the WMT is supported by recently published geophysical data that revealed the modern crust of WMT has a total thickness of about 30 km (Wang et al., 2019b; Zhang et al., 2021a). Paleocene to Pliocene sedimentary sequences in the fore-arc basin west of the WPA has a total thickness over 10 km (Htut, 2017) consistent with crustal scale 3-D seismic velocity models (Wang et al., 2019b). After removing the upper crustal sequence of post-Cretaceous sediments this suggest that the crust of the WMT during the Cretaceous was about 20 km (see Fig. A3 of Morley et al., 2020) similar to that of the Mariana arc (Takahashi et al., 2007). Moreover, P wave velocity imaging of an *E*-W trending cross-section at N24° showing the *Vp* is of 6.5 km/s at around 20 km and gradually increase to 8.0 km/s at >50 km depth (Fig. S4, produced with seismic data of Zhang et al., 2021a), is fairly consistent with intra-oceanic arcs elsewhere (Jagoutz and Kelemen, 2015).

In summary, available data show no Precambrian magmatic, metamorphic and sedimentary rocks in the WMT, which, along with depleted Nd-Hf isotopic compositions and the mantle-like zircon O isotopes of Cretaceous magmatic rocks (Gardiner et al., 2018) are consistent with a juvenile crustal origin for the WMT, and that it formed as an intra-oceanic arc (this study, Westerweel et al., 2019; Licht et al., 2020; Zhang et al., 2021b).

5.2. *Petrogenesis of the mid-Cretaceous BKC*

5.2.1. *The mafic and dioritic rocks*

The effect of crustal contamination needs to be evaluated before further investigation of the petrogenesis. Because continental crust generally displays higher Th/La, Th/Nd, initial $^{87}Sr/^{86}Sr$ values, but lower Nb/La and εNd(t) values than those of normal mid-ocean ridge basalt (N-MORB), positive correlation of ($^{87}Sr/^{86}Sr$)i and Th/La, εNd(t) and Nb/La would be expected if the magmas were contaminated by continental crust, but these are not observed in gabbros from the BKC and basalts from the Mawgyi Volcanics (Fig. 7a, b), indicating limited crustal contamination. It is also supported by the scatter of Nb/La and Th/Nb ratios within the wide range of MgO contents (Fig. 7c, d).

Mafic rocks analyzed in this study have MgO contents (4.29–7.21 wt %) and Mg# (46–65) lower than normal mantle-derived primary

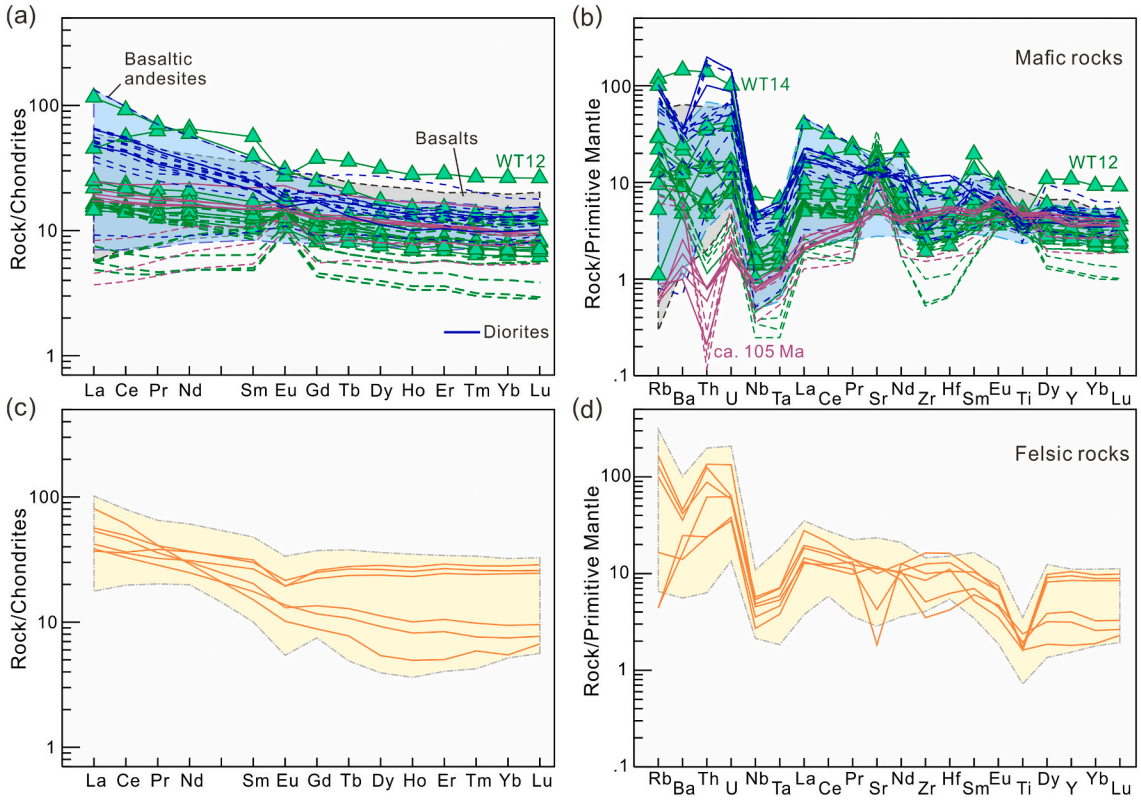

Fig. 4. (a and c) are Chondrite-normalized REE, (b, d) are primitive mantle-normalized trace elements spidergrams of the rocks from the BKC. Purple lines refer to ca. 105 Ma basalts of Mawgyi Volcanics (solid, Zhang et al., 2021b) and gabbros from BKC (dashed, this study, Li et al., 2020), respectively. Green lines refer to the remaining gabbros from BKC (Solid, this study; dashed, Li et al., 2020). Blue lines denote diorites of the BKC (This study, Li et al., 2020; Licht et al., 2020). Chondrite and primitive mantle normalizing values are from Sun and McDonough Sun and McDonough (1989). (For interpretation of the references to colour in this figure legend, the reader is referred to the web version of this article.) (For interpretation of the references to colour in this figure legend, the reader is referred to the web version of this article.)

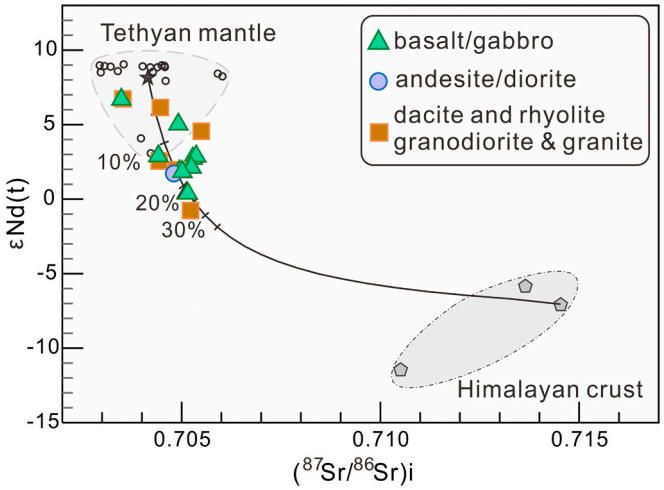

Fig. 5. Nd-Sr isotope diagrams for the BKC. Data source: Himalayan crust from Dai et al. (2008) and Zeng et al. (2011); Tethyan mantle values from Zhang et al. (2005).

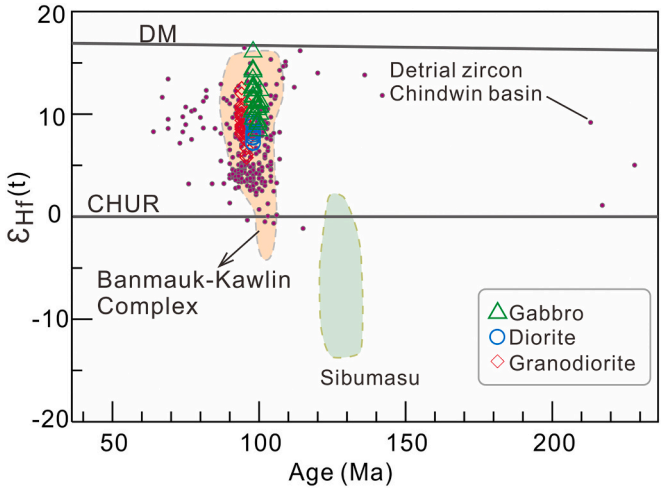

Fig. 6. Zircon Hf isotope vs. ages plots for the samples from BKC in Myanmar. Detrital zircons of the Upper Cretaceous Kabaw Formation and Paleocene Paunggyi Formation (dot) are from the fore-arc basin (Wang et al., 2014b); data of the Banmauk-Kawlin complex are from (Gardiner et al., 2017; Li et al., 2020; Lin et al., 2019; Zhang et al., 2017), and the field of magmatic rocks in Sibumasu is after Li et al. (2020) and references therein.

magmas (Herzberg and O'Hara, 2002). The low Cr, Ni contents and positive correlations between CaO, CaO/Al_2O_3 and MgO contents (Fig. S5), indicate fractionation of olivine and clinopyroxene. Plagioclase accumulation could be significant for some gabbros as indicated by their variable Eu anomalies (Fig. 4a, Eu/Eu* ups to 1.35) and high Al_2O_3 contents (<19.8 wt%). Given that the gabbros and volcanic rocks have similar REE and trace elements patterns (Fig. 4a, b), it is suggested plagioclase accumulation may not have significantly affected the trace element fingerprint.

The gabbro samples are characterized by enrichments in LILEs (e.g.,

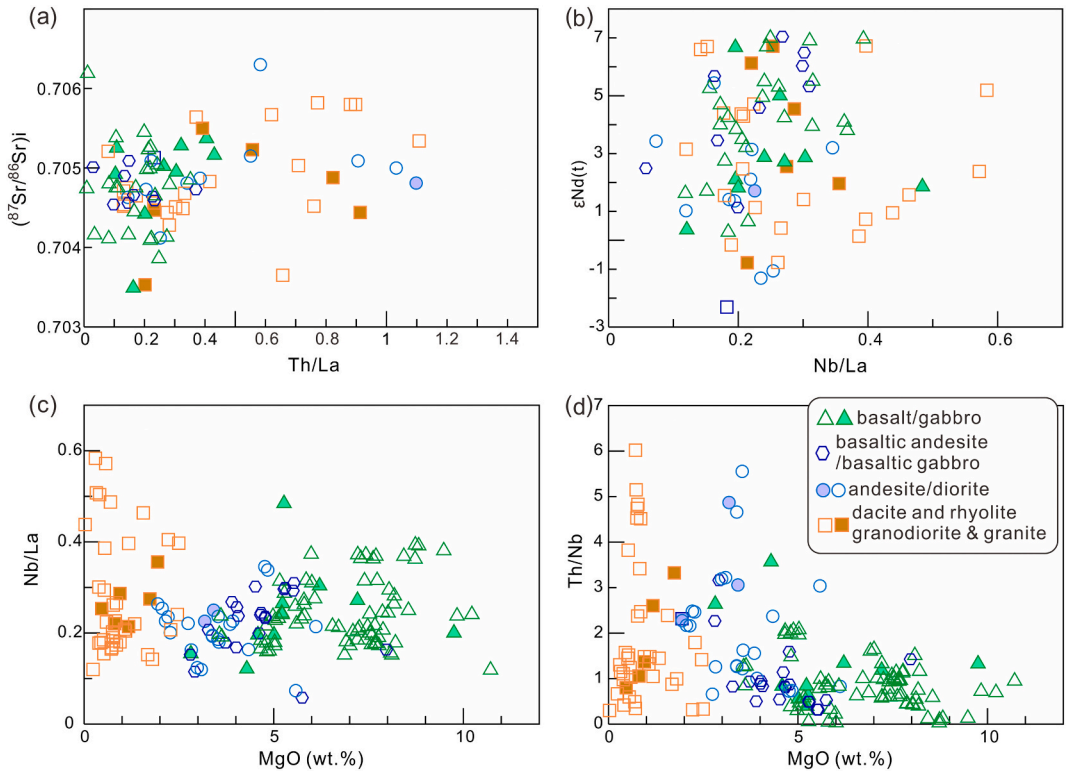

Fig. 7. Plots of (a) whole-rock $(^{87}Sr/^{86}Sr)_i$ vs. Th/La, (b) εNd(t) vs. Nb/La, (c-d) Nb/La and Th/Nb ratios vs. MgO.

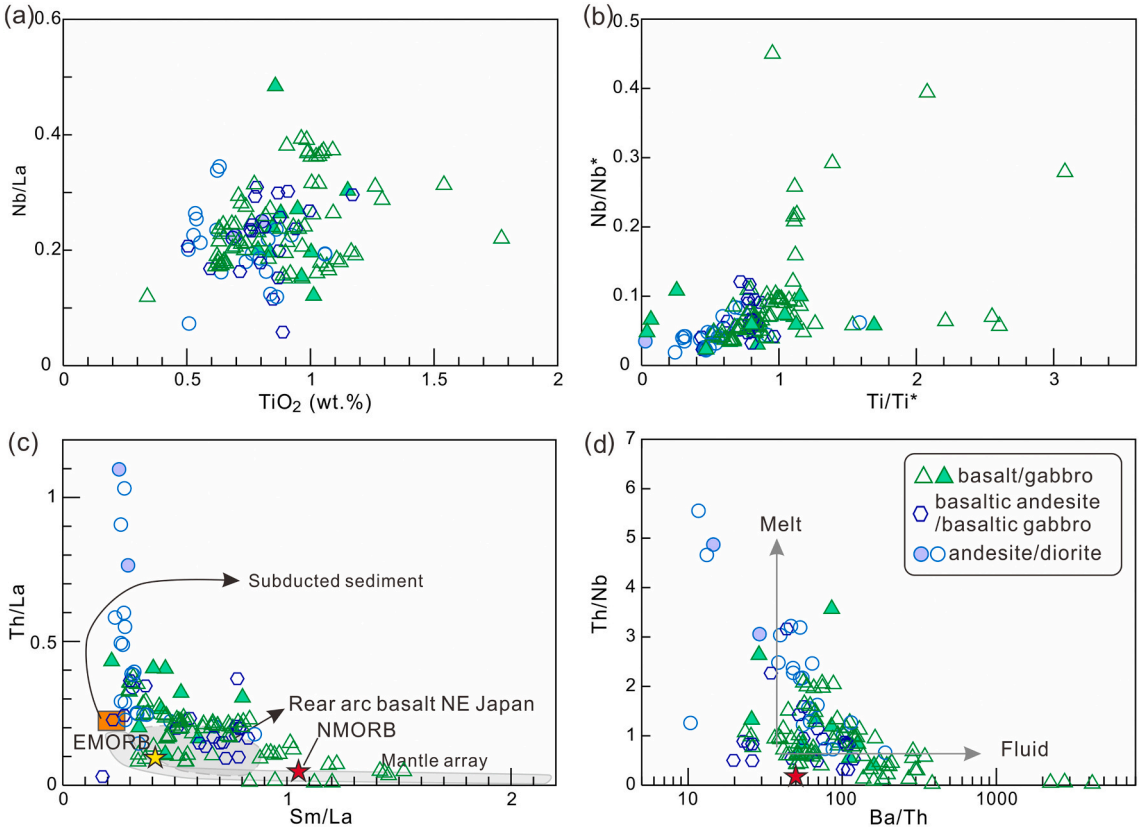

Fig. 8. Plots of (a) Nb/La vs. TiO_2. (b) Nb/Nb* (Primitive mantle normalized value, 0.618 × Nb /sqrt(Th × La)) vs Ti/Ti* (Primitive normalized value, Ti / ($Nd^{-0.055}$ × $Sm^{0.333}$ × $Gd^{0.722}$)). (c) Th/La vs. Sm/La (Kimura and Yoshida, 2006). (d) Tb/Nb vs. Ba/Th (George and Rogers, 2002).

Ba, Th) and LREE and depletions in HFSEs (e.g., Nb, Zr, Ti), typical of arc-like rocks (Kelemen et al., 2014). As demonstrated above, crustal contamination is negligible and the absence of significant correlations between Nb/La and TiO_2 (Fig. 8a), and between Nb and Ti anomalies (Fig. 8b) collectively suggests the depletions of HFSEs could not have resulted from fractional crystallization of Fe-Ti oxides. Therefore, the geochemical signals are best interpreted as indicating that the rocks formed in a supra-subduction zones setting.

The Tethyan mantle had distinctively high radiogenic Nd isotopes with $\varepsilon_{Nd}(t)$ values mostly around +8 (Xu and Castillo, 2004; Zhang et al., 2005). The gabbros from BKC have depleted Nd isotopic compositions (εNd(t): 0.28 to 6.67), shifting off the Tethyan mantle field (Fig. 5). Their enrichments in LILEs and depletions in Nb-Ta, and weakly radiogenic Nd isotope data are consistent the mantle regions that were metasomatized by a subduction component (Kelemen et al., 2014) given the lack of evidence for crustal contamination described above. High Th/La and Th/Nb for Cretaceous mafic rocks in central Myanmar (Fig. 8c, d) imply an input of sediment-derived melt. The high Th/U ratios (2.38–9.75) are analogous to those of subducted sediments (Plank and Langmuir, 1998) and also lavas from Merapi Volcano, Central Java which has been interpreted to have been derived from a mantle source that was strongly metasomatized by subducted sediment melts (Gertisser and Keller, 2003). On the plots of zircon Hf isotope vs. bulk-rock Nd isotope, the <103 Ma gabbros plot above and deviate away from the terrestrial array (Fig. 9; Vervoort et al., 2011), consistent with involvement of sediments or continent-derived components (Wang et al., 2014a). Strontium-Nd and Hf-Nd isotope mixing models suggest that about 10–20% sediment melts were incorporated in to the mantle wedge source (Figs. 5 and 9).

Diorites from the BKC could be generated by fractionation of parental magmas associated with gabbros. This is supported by their lower MgO, Fe_2O_3t, CaO contents relative to the basaltic rocks (Fig. S3a-c). They have higher incompatible element concentrations than those of most gabbros (Fig. 4a, b), consistent with the diorites being residual melts after fractional crystallization. Furthermore, the diorites are coeval with gabbros and have similar Nd isotopes as those mafic rocks (Fig. 5). Taken together, the diorites most likely originated from the fractionated melts of mantle-derived basaltic magmas.

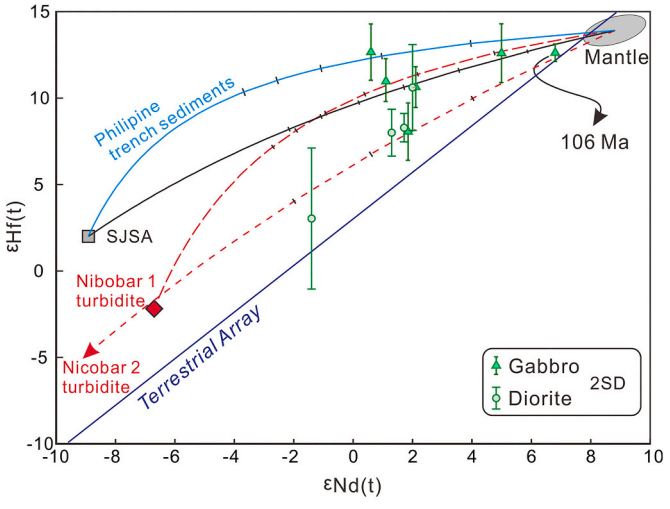

Fig. 9. Zircon εHf(t) vs. whole-rock εNd(t) plots for magmatic rocks of the BKC. The terrestrial array and Nicobar turbidites are from Vervoort et al. (2011); the mantle values (Nd: 7.120, Hf: 1.189) are from Xu and Castillo (2004) and isotopic values (εNd(t): 8.8, εHf(t): 13.9) are from Chauvel et al. (2008); the Hf and Nd element contents of SJSA (average of Sunda, Java, Sumatra, and Andaman trench sediments) and Philippine trench sediments are from Plank and Langmuir (1998), the corresponding isotopes are from Chauvel et al. (2008). Tick marks are 5% increments of the endmember.

5.2.2. Formation of the felsic rocks

Felsic rocks including granodiorites and minor granites constitute a major part of the BKC. Evolved rocks with high silica are unlikely to have formed directly by the partial melting of mantle. Crystal fractionation of mafic magmas also seems unlikely, as the amount of outcrop of coeval basaltic and intermediate rock is significantly less than the felsic phases (e.g., Atherton and Petford, 1993).

The felsic rocks from BKC could have formed by remelting of basaltic rocks with low potassium contents (Winther and Newton, 1991). Experimental data show that melts of common crustal material are primarily the function of source characteristics (Roberts and Clemens, 1993). Therefore, low- to middle-K_2O series granitic rocks from the BKC (Fig. 3c-d) were likely derived from a magma source with low K_2O. This is consistent with experimental melts of basaltic and andesitic rocks with low K_2O contents (<0.4 wt%) at crustal pressures (Beard and Lofgren, 1991). In contrast, glasses produced by melting of basaltic starting materials with $K_2O > 1.0$ wt% are similar to typical granites (Sisson et al., 2005).

Two-mica granites from the Pinhinga plutonic complex are Na-enriched, yielded zircon U-Pb age of ca. 102–98 Ma with depleted zircon Hf isotopes similar to granitoids from the Kanza Chaung batholith (Lin et al., 2019). Their Na_2O enrichment is unlike K_2O-enriched two-mica granites in Himalaya, which are generally derived from metasedimentary rocks (Ma et al., 2017; King et al., 2011). The Na_2O-enriched two-mica granites are associated with diorite, granodiorite, and small leucocratic granite (Mitchell, 2018). Though the genetic relationship between the various phases is poorly constrained, the rock associations of the Pinhinga complex implies that the strongly peraluminous melts were likely generated by extensive fractionation of less evolved parental magmas, possibly equivalents of the dioritic to granodioritic magmas (e.g., Ma et al., 2017; Zhang et al., 2021c). Felsic rocks have been identified in the modern Izu-Bonin-Mariana arc, including tonalitic to rhyolitic rocks (Tamura and Tatsumi, 2002; Tani et al., 2010); medium-K granodiorites contain biotite with enriched LILEs and LREEs are also reported from the Daisan West Sumisu knoll in the Izu arc (Tani et al., 2015). These observations show that granitic rocks can be formed in an intra-oceanic arc.

In summary, the gabbros with arc basaltic compositions originated from partial melting of a mantle wedge that was metasomatized by slab sediment-derived melts (Kelemen et al., 2014; Woodhead et al., 2001). Dioritic magmas formed mainly through differentiation of mantle-derived mafic magmas (Lee and Bachmann, 2014). With the introduction of heat and water source from fractionation of parental basaltic liquids, melting early basaltic rocks and generation of granitic magmas is predictable (Atherton and Petford, 1993; Winther and Newton, 1991).

6. Tectonic implications

6.1. A mid-Cretaceous collision event

Various rocks from the Kanza Chaung batholith and the Mawgyi Volcanic rocks show a shift in εNd(t) values from around +7 at ca. 105 Ma to zero at ca. 94 Ma (Fig. 10a). The shift to lower rock εNd(t) values in the granodiorites and more evolved rocks from the Kanza Chaung batholith and Mawgyi Volcanics are probably not the result of reworking of ancient continental crust given that evidence for ancient crust material beneath the WMT is elusive. Moreover, two-mica granites in north Banmauk are characterized by positive whole-rock $\varepsilon_{Nd}(t)$ values and Na_2O-enrichment (Licht et al., 2020) consistent with the absence of ancient crustal material beneath central Myanmar. Furthermore, Mitchell (1986) proposed that the Mawgyi Volcanics was a west-verging oceanic nappe and emplaced from east, whereas no structural evidence supports this model (Barber et al., 2017). Considering the large overlap of zircon U-Pb ages (This study, Li et al., 2020; Licht et al., 2020; Zhang et al., 2021b) and the intrusive contact between the BKC and the Mawgyi Volcanic rocks (Mitchell, 1993), the volcanic sequences were

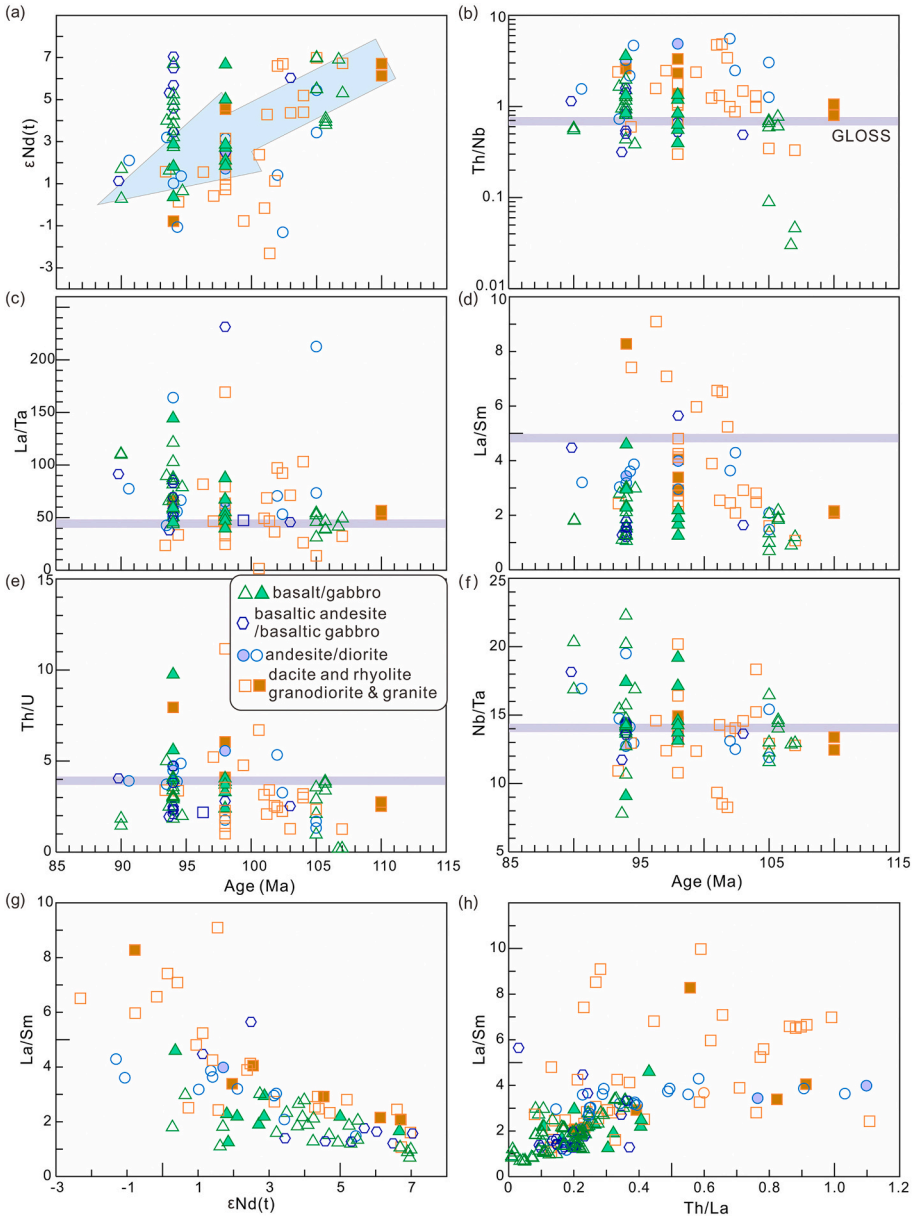

Fig. 10. Plots (a–h) of bulk-rock Nd isotopes, Th/Nb, La/Ta, La/Sm, Th/U, and Nb/Ta vs. age, respectively. The negative correlation of La/Sm and rock Nd isotopic compositions (g), and positive correlation between the La/Sm and Th/La (h) indicate sediment involvement. Global subducting sediment (GLOSS, purple band) are from Plank and Langmuir (1998). The open symbols represent data from (Li et al., 2020; Licht et al., 2020; Zhang et al., 2021b). (For interpretation of the references to colour in this figure legend, the reader is referred to the web version of this article.)

autochthonous.

The temporal shift of εNd(t) values is also significant for mafic rocks from the Kanza Chaung batholith and the Mawgyi Volcanic rocks (Fig. 10a). The Cretaceous Kabaw Formation and Paleocene Paunggyi Formation sediments from the fore-arc basin west of the WPA also exhibit an obvious negative excursion in zircon εHf(t) values at 103–97 Ma (Fig. 6; Wang et al., 2014b). Dominantly volcanic detritus, young ages (mostly <200 Ma), and depleted zircon Hf isotopes suggest that the WPA might be the predominant provenance contributor to these basins (Wang et al., 2014b). Given the lack of ancient basement in the WMT (e.g., Gardiner et al., 2018; Licht et al., 2020), the addition of exotic isotopically enriched component into mantle source region is necessary. Such exotic material could be introduced by either oceanic slab subduction or arc/continent-continent collision.

Secular and steady-state sediment subduction cannot explain such an abrupt Nd isotopic excursion, as it should lead to gradual enrichment of the mantle source region. Similarly, the large variation of zircon εHf(t) values (17 units, Gardiner et al., 2017; Li et al., 2020; Lin et al., 2019; Zhang et al., 2017) of the ~100 Ma magmatic rocks in the WPA cannot be explained by sediment subduction (e.g., Chu et al., 2011). Most gabbros of the BKC exhibit lower La/Sm (1.65–2.94) values than the marine sediments (generally >3, Plank and Langmuir, 1998). High contributions of marine sediments into the mantle source would result in mafic rocks with heavy oxygen isotope, high initial $^{87}Sr/^{86}Sr$ ratio, and elevated K_2O (e.g., Gertisser and Keller, 2003; Wang et al., 2014a). These contrast with the mantle-like zircon $\delta^{18}O$ values (Gardiner et al., 2018), low- to middle-K_2O calc-alkaline characteristics, and low initial $^{87}Sr/^{86}Sr$ ratios (This study, Li et al., 2020; Zhang et al., 2021b) for the BKC. In addition, according to the most recent paleomagnetic data (Westerweel et al., 2019), the WMT was an intra-oceanic arc at ca. 100 Ma. Due to the long distance away from continent, recycling of isotopically enriched sediments (e.g., continental clastic materials) into the mantle should be relatively limited (e.g., Draut and Clift, 2001). Therefore, the negative shift of the εNd(t) values for the BKC is likely related to arc/continent-continent collision. This is similar to chemical evolution observed in other well documented collision events, such as the Indo-Asia welding and the British South Mayo Lough Nafooey arc converging with Laurentia (Bouilhol et al., 2013; Chu et al., 2011; Draut and Clift, 2001).

Geochemical evolution of the Cretaceous BKC and adjacent volcanic

rocks is consistent with the collision hypothesis above. Continental collision commonly involves the subduction of continental crust following oceanic slab subduction (Chu et al., 2011; Elburg et al., 2004). Mafic rocks formed at ca. 105 Ma display trace patterns different from younger igneous rocks (<100 Ma; Fig. 4b; Li et al., 2020; Licht et al., 2020; Zhang et al., 2021b). The BKC show appreciable temporal trends of several trace ratios (Fig. 10b-f). Their Th/Nb, La/Ta, La/Sm, and Th/U increased from ca. 105 to 94 Ma. The good correspondence between their high Th/Nb, La/Ta, and Th/U ratios and large variation of Nb/Ta values of the ca. 94 Ma basaltic rocks is consistent with involvement of continental crust material (Goss and Kay, 2009). Because crustal contamination during magma ascent is negligible, the La/Sm ratios of the BKC exhibit negative correlation with whole-rock εNd(t) values (Fig. 10g), and positively correlate with Th/La values (Fig. 10h) also supports subduction of continental crust-derived sediment (e.g., Clift et al., 2002; Draut and Clift, 2001).

The angular unconformity observed on the WMT further supports such a collision event and crustal uplift. This unconformity can be loosely constrained to the Carnian–Albian interval, as indicated by observations that basaltic lavas and Carnian turbidites were unconformably covered by basal conglomerate and Albian-Cenomanian limestones in the east Mt. Voctoria area (Acharyya, 2015; Mitchell, 1993), east Chindwin basin (Barber and Crow, 2009; Morley, 2012), and the Tagaung-Myitkyina area (Mitchell et al., 2007). Though an accurate timing for the unconformity is lacking, it should be between ~113 and 100 Ma (Albian). The timing of Nd isotopes excursion for the BKC could better constrain the collision event to 105–94 Ma. Mitchell (1986) has proposed a collision between a Gondwana derived block with Triassic flysch and an obducted 'Kalaymyo' ophiolite nappe in the latest Jurassic. Zircon U-Pb ages of ca. 125 Ma for rodingites and ca. 115 Ma for amphibolites in the Kalaymyo ophiolite (Liu et al., 2016), and the Late Jurassic (Kimmeridgian-early Tithonian) radiolarian cherts from Nagaland ophiolite (Baxter et al., 2011), collectively suggest that the oceanic basin represented by the Kalaymyo ophiolite was not closed in the Early Cretaceous. That is, the collision event should occur later than ca. 115 Ma.

Other independent geological evidence includes Aptian-Albian basin subsidence, which was suggested to be related to a mid-Cretaceous collision (Morley, 2012). Strongly peraluminous two-mica granites in the Pinhinga Plutonic complex (Mitchell, 2018; United Nations, 1978 and references therein) north of the Banmauk area have zircon U-Pb ages of ca. 100 Ma (Lin et al., 2019), broadly contemporaneous with the Kanza Chaung batholith (This study, Li et al., 2020; Licht et al., 2020). These typical crustal source-derived magmas are commonly considered to be related to continental collision (Harris et al., 1986; Le Fort, 1981). Collision-related orogenic collapse in the Late Cretaceous is consistent with a collision event during the mid-Cretaceous, which has been identified in the WMT and adjacent areas (Mitchell, 2018; Zhang et al., 2017). The Upper Cretaceous sedimentary sequences in the eastern WPA show typical rifting structure and negative flower structures on two *E*-W trending seismic profiles (at latitudes of approximate N22°30′ and N23°30′) across the WPA and the back-arc basin (Zhang et al., 2017). In addition, the metamorphic core complex in the Mogok area also supports crustal extension (Mitchell, 1993). In combination, the Nd isotope negative shift for the mid-Cretaceous BKC in Myanmar could be related to a collisional event.

6.2. Broader implications

The formation of the mid-Cretaceous BKC has been suggested to be related to a collisional event. The Sibumasu terranes to the east or small continental strip to the west are the two potential candidates to collide with the WMT, and these will be tested with available data below.

Ultra-mafic and mafic rocks in the Myitkyina area have been suggested to be relict oceanic lithosphere, and are the southward extension of the Meso-Tethys Suture Zone in Tibet (Liu et al., 2016). However, recent magmatic, structural, and sedimentary data suggest that the final closure of the Meso-Tethys Ocean in Tibet was in the Early Cretaceous (~130 Ma; Li et al., 2019b), significantly predating the formation of BKC. In other words, due to their arc-like features (Xu et al., 2017) and the absence of a closely related fore-arc accretionary complex (Zhang et al., 2018), it is more likely that they were associated with Neo-Tethys subduction (Mitchell, 2018; Zhang et al., 2018). Therefore, a mid-Cretaceous collision between the Sibumasu terrane and the WMT seems unlikely, whereas accretion of the WMT to the west of Sibumasu could have occured at ca. 45 Ma (Licht et al., 2020). This is supported by the paleolatitude of the WMT (Westerweel et al., 2019), palynological patterns (Huang et al., 2021), and the abrupt increase in ancient detritus during mid-Eocene (Wang et al., 2014b). This collision probably caused the ca. 45 Ma high-grade metamorphism in the Mogok area (Searle et al., 2020).

Multiple independent lines of evidence indicate continental crust of

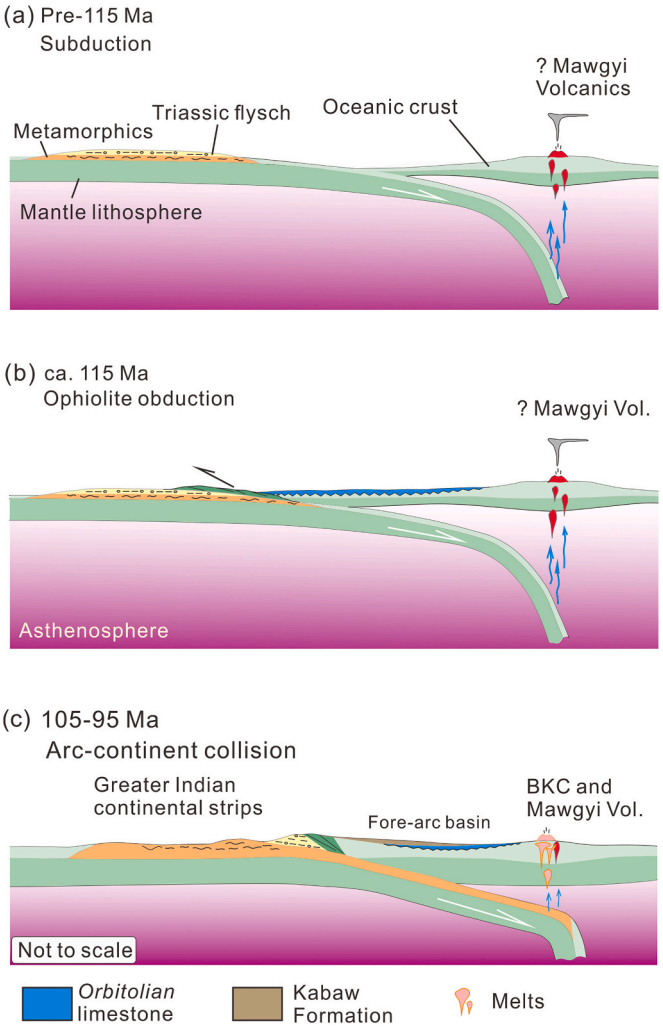

Fig. 11. Tectonic model illustrating the generation of the BKC, Myanmar. (a) Arc magmas were generated prior to ca. 115 Ma associated with oceanic slab subduction, possibly an early phase of the Mawgyi Volcanics. (b) Ophiolite obduction onto the Carnian flysch in IBR, roughly coeval with the angular unconformity below the Upper Albian-Cenomanian *Orbitolian*-bearing limestone and its basal conglomerate. (c) During the mid-Cretaceous, isotopically enriched crust, possibly continental fragments derived from Greater India collided with the WMT and descended into mantle source of the BKC. Exhumation and erosion of the BKC and Mawgyi Volcanics provide volcanogenic detritus for the later sequences, such as the Kabaw Formation and Paunggyi formation. The collision position is constrained by the paleomagnetic data of van Hinsbergen et al. (2019) and Westerweel et al. (2019).

Indian affinity to the west (at current coordinates) collided with the WMT in the mid-Creataceous (e.g., Fig. 11). In the Mt. Victoria Land area within the IBR, the Late Triassic Pane Chaung Formation and underlying Kampetlet Schists (Morley et al., 2020) are unconformably sealed by Albian limestone (Acharyya, 2015; Mitchell, 1993). Based on the analogue between the Tethyan Himalayan sequences (e.g., the Langjiexue Group in Tibet) and the Pane Chaung Formation with regard to fossils, sedimentary provenance, and diagnostic 200–300 Ma zircon populations (Cai et al., 2019; Wang et al., 2016; Yao et al., 2017), it is reasonable to infer the Triassic Pane Chaung Formation was equivalent to (or part of) the Tethyan Himalayan sequences. This continental ribbon likely separated from Gondwana (Mitchell, 1986) and drifted northward, coinciding with the Early Cretaceous extensional event in Tethyan Himalaya (Ma et al., 2018). The abrupt bulk-rock Nd isotopic enrichment of BKC gabbros could due to input of crustal materials similar to the Tethyan Himalayan sequences, which were isotopically enriched (King et al., 2011; Ma et al., 2018; Zeng et al., 2011).

Newly published paleomagnetic data suggests the WMT was located at around 5°S ± 5° in ~100 Ma (Fig. S6, Westerweel et al., 2019), and the WMT was an intra-oceanic arc associated with the Trans-Tethyan subduction zone (Licht et al., 2020; Morley et al., 2020; Zhang et al., 2021b). In the Greater Indian Basin scenario (van Hinsbergen et al., 2012), the Tethyan Himalaya was moving northward much faster than remaining of the India continent, implying remarkable extension and oceanic basin formation (van Hinsbergen et al., 2012, 2019). It is suspected that this period of extension resulted from the onset of the Kerguelen mantle plume (Zhu et al., 2009), as indicated by the Comei-Bunbury large igneous province (~130 Ma) in the Tethyan Himalaya (Ma et al., 2018; Zhu et al., 2009). During the same time, some microcontinental terranes (fragments?), possibly equivalents to (or part of) the Tethyan Himalaya, could rift and drift rapidly northward away from the Greater India, and ultimately collide with the WMT in the mid-Cretaceous (e.g., Morley et al., 2020). This collision was predicted when a moderate plate motion rate was assumed according to Early Cretaceous paleomagnetic data from Tethyan Himalaya (Fig. S6, van Hinsbergen et al., 2012). On the whole, the temporal Nd isotope excursion in the BKC of Myanmar provides evidence that an India-derived continental fragment collided with the WMT at ca. 100–94 Ma (Fig. 11).

Geochemical trends of the Dras 1 and Khardung volcanics in the Kohistan arc (Pakistan) record a collision event (Clift et al., 2002), which was possibly related to the Late Cretaceous–Paleocene accretion of the Trans-Tethyan subduction zone onto India and is also supported by recent paleomagnetic and zircon U-Pb dating results (Martin et al., 2020). If the proposed mid-Cretaceous collision between the intra-oceanic arc (WMT) and Greater India-derived continental ribbon did occur, the initial approach of the India-affinity crust could be as early as ~100 Ma. This collision could be partly the cause of the major clockwise rotation of the WMT after 95 Ma (Westerweel et al., 2019). In addition, available data concerning the Cretaceous magmatic rocks in central Myanmar provide new constraints on the multistage processes of the India-Eurasia collision (e.g., Martin et al., 2020).

7. Conclusions

Newly obtained data and other independent geological observations from Myanmar allow us to conclude:

1. The mid-Cretaceous arc-like mafic rocks in Myanmar were formed by partial melting of mantle metasomatized by subduction components;
2. The abrupt excursion in Nd isotope at ca. 100 Ma is mostly likely a consequence of the collision between the West Myanmar and India-derived continental strip.

Supplementary data to this article can be found online at https://doi.org/10.1016/j.lithos.2022.106637.

Declaration of Competing Interest

The authors declare no competing interest.

Acknowledgments

This work was jointly funded by the project of “Innovative Team of One Belt and One Road” of the Chinese Academy of Sciences, the National Natural Science Foundation of China (91955209, 42073047, 41673049), Hundred Talent Plan of the Chinese Academy of Sciences to Jing-Jing Zhu, and the project under the Frontier Programme of the State Key Laboratory of Ore Deposit Geochemistry, K.C. Wong Education Foundation (GJTD-2020-13), and China Postdoctoral Science Foundation (grant No. 2019M663572). The authors thank Yang Shuqin, Qi Liang, and Hu Jing for their assistance with bulk-rock geochemical analyses, and Dr. Tang Yan-Wen and Master student Jinkun Yang for zircon U-Pb and Hf isotope measurements. Prof. Jeremy Richards from Laurentian University Canada, who was Jing-Jing’s post-doctoral supervisor and passed away in June of 2019, encouraged Jing-Jing Zhu to initial this project and write this contribution. We dedicate this paper to his memory. Three anonymous reviewers and the Lithos’ editor Xian-Hua Li are thanked for their constructive comments that significantly improved the manuscript. Thanks to Prof. Ai Yinshuang (Institute of Geology and Geophysics, Chinese Academy of Sciences) for his gracious help providing the seismic data of Myanmar. Prof. Pete Hollings is thanked for help polishing the English of this paper.

References

Acharyya, S.K., 2015. Indo-Burma Range: a belt of accreted microcontinents, ophiolites and Mesozoic-Paleogene flyschoid sediments. Int. J. Earth Sci. 104, 1235–1251.
Aitchison, J.C., Ao, A., Bhowmik, S., Clarke, G.L., Ireland, T.R., Kachovich, S., Lokho, K., Stojanovic, D., Roeder, T., Truscott, N., Zhen, Y., Zhou, R., 2019. Tectonic evolution of the Western margin of the Burma microplate based on new fossil and radiometric age constraints. Tectonics 38, 1718–1741.
Atherton, M.P., Petford, N., 1993. Generation of sodium-rich magmas from newly underplated basaltic crust. Nature 362, 144–146.
Barber, A.J., Crow, M.J., 2009. Structure of Sumatra and its implications for the tectonic assembly of Southeast Asia and the destruction of Paleotethys. Island Arc 18, 3–20.
Barber, A., Zaw, K., Crow, M.J., 2017. Chapter 31 The pre-Cenozoic tectonic evolution of Myanmar. In: Barber, A.J., Zaw, K., Crow, M.J. (Eds.), Myanmar: Geology, Resources and Tectonics. Geological Society of London, London, pp. 687–712.
Barley, M.E., Pickard, A.L., Zaw, K., Rak, P., Doyle, M.G., 2003. Jurassic to Miocene magmatism and metamorphism in the Mogok metamorphic belt and the India-Eurasia collision in Myanmar. Tectonics 22.
Baxter, A.T., Aitchison, J.C., Zyabrev, S.V., Ali, J.R., 2011. Upper Jurassic radiolarians from the Naga Ophiolite, Nagaland, Northeast India. Gondwana Res. 20, 638–644.
Beard, J.S., Lofgren, G.E., 1991. Dehydration melting and water-saturated melting of basaltic and andesitic greenstones and amphibolites at 1, 3, and 6. 9 kb. J. Petrol. 32, 465–501.
Bouilhol, P., Jagoutz, O., Hanchar, J.M., Dudas, F.O., 2013. Dating the India–Eurasia collision through arc magmatic records. Earth Planet. Sci. Lett. 366, 163–175.
Cai, F., Ding, L., Zhang, Q., Orme, D.A., Wei, H., Li, J., Zhang, J.E., Zaw, T., Sein, K., 2019. Initiation and evolution of forearc basins in the Central Myanmar depression. GSA Bull. 132, 1066–1082.
Chauvel, C., Lewin, E., Carpentier, M., Arndt, N.T., Marini, J.-C., 2008. Role of recycled oceanic basalt and sediment in generating the Hf–Nd mantle array. Nat. Geosci. 1, 64–67.
Chu, M.-F., Chung, S.-L., O’Reilly, S.Y., Pearson, N.J., Wu, F.-Y., Li, X.-H., Liu, D., Ji, J., Chu, C.-H., Lee, H.-Y., 2011. India’s hidden inputs to Tibetan orogeny revealed by Hf isotopes of Transhimalayan zircons and host rocks. Earth Planet. Sci. Lett. 307, 479–486.
Clegg, E.L.G., 1941. The cretaceous and associated rocks of Burma. Geol. Sur. India Mem. 74, 1–102.
Clift, P., Hannigan, R., Blusztajn, J., Draut, A., 2002. Geochemical evolution of the Dras–Kohistan Arc during collision with Eurasia: Evidence from the Ladakh Himalaya, India. Island Arc 11, 255–273.
Coogan, L.A., Wilson, R.N., Gillis, K.M., MacLeod, C.J., 2001. Near-solidus evolution of oceanic gabbros: insights from amphibole geochemistry. Geochim. Cosmochim. Acta 65, 4339–4357.
Dai, J., Yin, A., Liu, W., Wang, C., 2008. Nd isotopic compositions of the Tethyan Himalayan sequences in southeastern Tibet. Sci. China Ser. D Earth Sci. 51, 1306–1316.
Draut, A.E., Clift, P.D., 2001. Geochemical evolution of arc magmatism during arc-continent collision, South Mayo, Ireland. Geology 29, 543–546.

Elburg, M.A., van Bergen, M.J., Foden, J.D., 2004. Subducted upper and lower continental crust contributes to magmatism in the collision sector of the Sunda-Banda. Geology 32, 41–44.
Enami, M., Zaw Win, K., Aung, W., Tsuboi, M., 2012. Eclogite from the Kumon range, Myanmar: Petrology and tectonic implications. Gond. Res. 21, 548–558.
Gardiner, N.J., Hawkesworth, C.J., Robb, L.J., Whitehouse, M.J., Roberts, N.M.W., Kirkland, C.L., Evans, N.J., 2017. Contrasting granite metallogeny through the zircon record: a case study from Myanmar. Sci. Rep. 7, 748.
Gardiner, N.J., Searle, M.P., Morley, C.K., Robb, L.J., Whitehouse, M.J., Roberts, N.M.W., Kirkland, C.L., Spencer, C.J., 2018. The crustal architecture of Myanmar imaged through zircon U-Pb, Lu-Hf and O isotopes: Tectonic and metallogenic implications. Gondwana Res. 62, 27–60.
George, R., Rogers, N., 2002. Plume dynamics beneath the African plate inferred from the geochemistry of the Tertiary basalts of southern Ethiopia. Contrib. Mineral. Petrol. 144, 286–304.
Gertisser, R., Keller, J., 2003. Trace element and Sr, Nd, Pb and O isotope variations in medium-K and high-K volcanic rocks from Merapi Volcano, Central Java, Indonesia: evidence for the involvement of subducted sediments in Sunda Arc Magma genesis. J. Petrol. 44, 457–489.
Goss, A.R., Kay, S.M., 2009. Extreme high field strength element (HFSE) depletion and near-chondritic Nb/Ta ratios in Central Andean adakite-like lavas (~ 28°S, ~ 68°W). Earth Planet. Sci. Lett. 279, 97–109.
Harris, N.B., Pearce, J.A., Tindle, A.G., 1986. Geochemical characteristics of collision-zone magmatism. Geol. Soc. Lond., Spec. Publ. 19, 67–81.
Herzberg, C., O'Hara, M.J., 2002. Plume-associated ultramafic magmas of phanerozoic age. J. Petrol. 43, 1857–1883.
Hoskin, P.W.O., Schaltegger, U., 2003. The composition of zircon and igneous and metamorphic petrogenesis. Rev. Mineral. Geochem. 53, 27–62.
Htut, T., 2017. Chapter 11 Myanmar petroleum systems, including the offshore area. In: Barber, A.J., Zaw, K., Crow, M.J. (Eds.), Myanmar: Geology, Resources and Tectonics. Geological Society, London, Memoirs, pp. 219–260.
Hu, Z., Liu, Y., Gao, S., Liu, W., Zhang, W., Tong, X., Lin, L., Zong, K., Li, M., Chen, H., Zhou, L., Yang, L., 2012. Improved in situ Hf isotope ratio analysis of zircon using newly designed X skimmer cone and jet sample cone in combination with the addition of nitrogen by laser ablation multiple collector ICP-MS. J. Anal. At. Spectrom. 27, 1391–1399.
Huang, H., Pérez-Pinedo, D., Morley, R.J., Dupont-Nivet, G., Philip, A., Win, Z., Aung, D. W., Licht, A., Jardine, P.E., Hoorn, C., 2021. At a crossroads: the late Eocene flora of Central Myanmar owes its composition to plate collision and tropical climate. Rev. Palaeobot. Palynol. 291, 104441.
Jagoutz, O., Kelemen, P.B., 2015. Role of arc processes in the formation of continental crust. Annu. Rev. Earth Planet. Sci. 43, 363–404.
Jagoutz, O., Royden, L., Holt, A.F., Becker, T.W., 2015. Anomalously fast convergence of India and Eurasia caused by double subduction. Nat. Geosci. 8, 475–478.
Ji, W.-Q., Wu, F.-Y., Chung, S.-L., Liu, C.-Z., 2014. The Gangdese magmatic constraints on a latest cretaceous lithospheric delamination of the Lhasa terrane, southern Tibet. Lithos 210-211, 168–180.
Kelemen, P.B., Hanghøj, K., Greene, A.R., 2014. 4.21 - One view of the geochemistry of subduction-related magmatic arcs, with an emphasis on primitive andesite and lower crust. In: Holland, H.D., Turekian, K.K. (Eds.), Treatise on Geochemistry (Second Edition). Elsevier, Oxford, pp. 749–806.
Kimura, J.-I., Yoshida, T., 2006. Contributions of Slab Fluid, Mantle Wedge and Crust to the Origin of Quaternary Lavas in the NE Japan Arc. J. Petrol. 47, 2185–2232.
King, J., Harris, N., Argles, T., Parrish, R., Zhang, H., 2011. Contribution of crustal anatexis to the tectonic evolution of Indian crust beneath southern Tibet. Geol. Soc. Am. Bull. 123, 218–239.
Le Fort, P., 1981. Manaslu leucogranite: a collision signature of the Himalaya: a model for its genesis and emplacement. J. Geophys. Res. Solid Earth 86, 10545–10568.
Lee, C.-T.A., Bachmann, O., 2014. How important is the role of crystal fractionation in making intermediate magmas? Insights from Zr and P systematics. Earth Planet. Sci. Lett. 393, 266–274.
Lee, H.-Y., Chung, S.-L., Yang, H.-M., 2016. Late Cenozoic volcanism in Central Myanmar: Geochemical characteristics and geodynamic significance. Lithos 245, 174–190.
Li, X.H., Long, W.G., Li, Q.L., Liu, Y., Zheng, Y.F., Yang, Y.H., Chamberlain, K.R., Wan, D. F., Guo, C.H., Wang, X.C., 2010. Penglai zircon megacrysts: A potential new working reference material for microbeam determination of Hf–O isotopes and U–Pb age. Geostand. Geoanal. Res. 34, 117–134.
Li, X.H., Tang, G.Q., Gong, B., Yang, Y.H., Hou, K.J., Hu, Z.C., Li, Q.L., Liu, Y., Li, W.X., 2013. Qinghu zircon: a working reference for microbeam analysis of U-Pb age and Hf and O isotopes. Sci. Bull. 58, 4647–4654.
Li, J.-X., Fan, W.-M., Zhang, L.-Y., Ding, L., Sun, Y.-L., Peng, T.-P., Cai, F.-L., Guan, Q.-Y., Sein, K., 2019a. Subduction of Indian continental lithosphere constrained by Eocene-Oligocene magmatism in northern Myanmar. Lithos 348-349, 105211.
Li, S., Yin, C., Guilmette, C., Ding, L., Zhang, J., 2019b. Birth and demise of the Bangong-Nujiang Tethyan Ocean: a review from the Gerze area of Central Tibet. Earth Sci. Rev. 198, 102907.
Li, J.-X., Fan, W.-M., Zhang, L.-Y., Peng, T.-P., Sun, Y.-L., Ding, L., Cai, F.-L., Sein, K., 2020. Prolonged Neo-Tethyan magmatic arc in Myanmar: evidence from geochemistry and Sr–Nd–Hf isotopes of Cretaceous mafic–felsic intrusions in the Banmauk–Kawlin area. Int. J. Earth Sci. 109, 649–668.
Licht, A., Win, Z., Westerweel, J., Cogné, N., Morley, C.K., Chantraprasert, S., Poblete, F., Ugrai, T., Nelson, B., Aung, D.W., Dupont-Nivet, G., 2020. Magmatic history of Central Myanmar and implications for the evolution of the Burma Terrane. Gondwana Res. 87, 303–319.
Lin, T.-H., Mitchell, A.H.G., Chung, S.-L., Tan, X.-B., Tang, J.-T., Oo, T., Wu, F.-Y., 2019. Two parallel magmatic belts with contrasting isotopic characteristics from southern Tibet to Myanmar: zircon U–Pb and Hf isotopic constraints. J. Geol. Soc. 176, 574–587.
Liu, Y., Hu, Z., Gao, S., Günther, D., Xu, J., Gao, C., Chen, H., 2008. In situ analysis of major and trace elements of anhydrous minerals by LA-ICP-MS without applying an internal standard. Chem. Geol. 257, 34–43.
Liu, C.-Z., Chung, S.-L., Wu, F.-Y., Zhang, C., Xu, Y., Wang, J.-G., Chen, Y., Guo, S., 2016. Tethyan suturing in Southeast Asia: Zircon U-Pb and Hf-O isotopic constraints from Myanmar ophiolites. Geology 44, 311–314.
Ma, L., Wang, Q., Wyman, D.A., Li, Z.-X., Jiang, Z.-Q., Yang, J.-H., Gou, G.-N., Guo, H.-F., 2013. Late cretaceous (100–89Ma) magnesian charnockites with adakitic affinities in the Milin area, eastern Gangdese: Partial melting of subducted oceanic crust and implications for crustal growth in southern Tibet. Lithos 175-176, 315–332.
Ma, L., Wang, Q., Kerr, A.C., Yang, J.-H., Xia, X.-P., Ou, Q., Yang, Z.-Y., Sun, P., 2017. Paleocene (c. 62 Ma) Leucogranites in Southern Lhasa, Tibet: Products of Syn-collisional Crustal Anatexis during Slab Roll-back? J. Petrol. 58, 2089–2114.
Ma, L., Kerr, A.C., Wang, Q., Jiang, Z.-Q., Hu, W.-L., 2018. Early cretaceous (~140Ma) aluminous A-type granites in the Tethyan Himalaya, Tibet: Products of crust-mantle interaction during lithospheric extension. Lithos 300-301, 212–226.
Martin, C.R., Jagoutz, O., Upadhyay, R., Royden, L.H., Eddy, M.P., Bailey, E., Nichols, C. I.O., Weiss, B.P., 2020. Paleocene latitude of the Kohistan–Ladakh arc indicates multistage India–Eurasia collision. Proc. Natl. Acad. Sci. 117, 29487.
Metcalfe, I., 2013. Gondwana dispersion and Asian accretion: Tectonic and palaeogeographic evolution of eastern Tethys. J. Asian Earth Sci. 66, 1–33.
Mitchell, A.H.G., 1986. Mesozoic and Cenozoic regional tectonics and metallogenesis in mainland SE Asia. Geol. Soc. Malaysia Bull. 20, 221–239.
Mitchell, A.H.G., 1993. Cretaceous-Cenozoic events in the western Myanmar (Burma) - Assam region. J. Geol. Soc. Lond. 150, 1089–1102.
Mitchell, A.H.G., 2018. Chapter 9 - Popa–Loimye magmatic arc. In: Geological Belts, Plate Boundaries, and Mineral Deposits in Myanmar. Elsevier, pp. 277–323.
Mitchell, A.H.G., McKerrow, W.S., 1975. Analogous evolution of the Burma orogen and the Scottish Caledonides. Geol. Soc. Am. Bull. 86, 305–315.
Mitchell, A.H.G., Htay, M.T., Htun, K.M., Win, M.N., Oo, T., Hlaing, T., 2007. Rock relationships in the Mogok metamorphic belt, Tatkon to Mandalay, Central Myanmar. J. Asian Earth Sci. 29, 891–910.
Mitchell, A.H.G., Chung, S.-L., Oo, T., Lin, T.-H., Hung, C.-H., 2012. Zircon U–Pb ages in Myanmar: Magmatic–metamorphic events and the closure of a neo-Tethys ocean? J. Asian Earth Sci. 56, 1–23.
Morley, C.K., 2012. Late Cretaceous–Early Palaeogene tectonic development of SE Asia. Earth Sci. Rev. 115, 37–75.
Morley, C.K., Tin Tin, N., Searle, M., Robinson, S.A., 2020. Structural and tectonic development of the Indo-Burma ranges. Earth Sci. Rev. 200, 102992 https://doi.org/10.1016/j.earscirev.2019.102992.
Peccerillo, A., Taylor, S.R., 1976. Geochemistry of Eocene calc-alkaline volcanic rocks from the Kastamonu area, Northern Turkey. Contrib. Mineral. Petrol. 58, 63–81.
Plank, T., Langmuir, C.H., 1998. The chemical composition of subducting sediment and its consequences for the crust and mantle. Chem. Geol. 145, 325–394.
Qi, L., Hu, J., Gregoire, D.C., 2000. Determination of trace elements in granites by inductively coupled plasma mass spectrometry. Talanta 51, 507–513.
Roberts, M.P., Clemens, J.D., 1993. Origin of high-potassium, talc-alkaline, I-type granitoids. Geology 21, 825–828.
Searle, M.P., Noble, S.R., Cottle, J.M., Waters, D.J., Mitchell, A.H.G., Hlaing, T., Horstwood, M.S.A., 2007. Tectonic evolution of the Mogok metamorphic belt, Burma (Myanmar) constrained by U-Th-Pb dating of metamorphic and magamtic rocks. Tectonics 26, TC3014.
Searle, M.P., Garber, J.M., Hacker, B.R., Htun, K., Gardiner, N.J., Waters, D.J., Robb, L.J., 2020. Timing of Syenite-Charnockite Magmatism and Ruby and Sapphire Metamorphism in the Mogok Valley Region. Myanmar. Tectonics 39, e2019TC005998.
Searle, M.P., Morley, C.K., Waters, D.J., Gardiner, N.J., Kyi Htun, U., Nu, T.T., Robb, L.J., Barber, A.J., Zaw, K., Crow, M.J., 2017. Tectonic and metamorphic evolution of the Mogok Metamorphic and Jade Mines belts and ophiolitic terranes of Burma (Myanmar). In: Barber, A.J., Zaw, K., Crow, M.J. (Eds.), Myanmar: Geology, Resources and Tectonics. The Geological Society of London, pp. 261–293.
Sisson, T., Ratajeski, K., Hankins, W., Glazner, A., 2005. Voluminous granitic magmas from common basaltic sources. Contrib. Mineral. Petrol. 148, 635–661.
Sláma, J., Košler, J., Condon, D.J., Crowley, J.L., Gerdes, A., Hanchar, J.M., Horstwood, M.S.A., Morris, G.A., Nasdala, L., Norberg, N., 2008. Plešovice zircon — A new natural reference material for U–Pb and Hf isotopic microanalysis. Chem. Geol. 249, 1–35.
Soesoo, A., 2000. Fractional crystallization of mantle-derived melts as a mechanism for some I-type granite petrogenesis: an example from Lachlan Fold Belt, Australia. J. Geol. Soc. Lond. 157, 135–149.
Sun, S.S., McDonough, W.F., 1989. Chemical and isotopic systematics of oceanic basalts: implications for mantle composition and processes. Geol. Soc. Lond., Spec. Publ. 42, 313.
Takahashi, N., Kodaira, S., Klemperer, S.L., Tatsumi, Y., Kaneda, Y., Suyehiro, K., 2007. Crustal structure and evolution of the Mariana intra-oceanic island arc. Geology 35, 203–206.
Tamura, Y., Tatsumi, Y., 2002. Remelting of an Andesitic crust as a possible origin for rhyolitic Magma in Oceanic Arcs: an example from the Izu–Bonin arc. J. Petrol. 43, 1029–1047.
Tani, K., Dunkley, D.J., Kimura, J.-I., Wysoczanski, R.J., Yamada, K., Tatsumi, Y., 2010. Syncollisional rapid granitic magma formation in an arc-arc collision zone: evidence from the Tanzawa plutonic complex, Japan. Geology 38, 215–218.

Tani, K., Dunkley, D.J., Chang, Q., Nichols, A.R.L., Shukuno, H., Hirahara, Y., Ishizuka, O., Arima, M., Tatsumi, Y., 2015. Pliocene granodioritic knoll with continental crust affinities discovered in the intra-oceanic Izu–Bonin–Mariana Arc: Syntectonic granitic crust formation during back-arc rifting. Earth Planet. Sci. Lett. 424, 84–94.

United Nations, 1978. Geology and Exploration Geochemistry of the Pinlebu-Banmauk Area, Sagaing Division, Northern Burma. Technical Report No.2, United Nations Development Programme, UN/BUR-72 002/6. United Nations, New York (69 p).

van Hinsbergen, D.J.J., Lippert, P.C., Dupont-Nivet, G., McQuarrie, N., Doubrovine, P.V., Spakman, W., Torsvik, T.H., 2012. Greater India Basin hypothesis and a two-stage Cenozoic collision between India and Asia. Proc. Natl. Acad. Sci. 109, 7659.

van Hinsbergen, D.J.J., Lippert, P.C., Li, S., Huang, W., Advokaat, E.L., Spakman, W., 2019. Reconstructing Greater India: Paleogeographic, kinematic, and geodynamic perspectives. Tectonophysics 760, 69–94.

Vervoort, J.D., Plank, T., Prytulak, J., 2011. The Hf–Nd isotopic composition of marine sediments. Geochim. Cosmochim. Acta 75, 5903–5926.

Wang, H., Wu, Y.-B., Li, C.-R., Zhao, T.-Y., Qin, Z.-W., Zhu, L.-Q., Gao, S., Zheng, J.-P., Liu, X.-M., Zhou, L., Zhang, Y., Yang, S.-H., 2014a. Recycling of sediment into the mantle source of K-rich mafic rocks: Sr–Nd–Hf–O isotopic evidence from the Fushui complex in the Qinling orogen. Contrib. Mineral. Petrol. 168, 1062.

Wang, J.-G., Wu, F.-Y., Tan, X.-C., Liu, C.-Z., 2014b. Magmatic evolution of the Western Myanmar Arc documented by U–Pb and Hf isotopes in detrital zircon. Tectonophysics 612-613, 97–105.

Wang, J.-G., Wu, F.-Y., Garzanti, E., Hu, X., Ji, W.-Q., Liu, Z.-C., Liu, X.-C., 2016. Upper Triassic turbidites of the northern Tethyan Himalaya (Langjiexue Group): the terminal of a sediment-routing system sourced in the Gondwanide Orogen. Gondwana Res. 34, 84–98.

Wang, J., Wang, Q., Dan, W., Yang, J.-H., Yang, Z.-Y., Sun, P., Qi, Y., Hu, W.-L., 2019a. The role of clinopyroxene in amphibole fractionation of arc magmas: evidence from mafic intrusive rocks within the Gangdese arc, southern Tibet. Lithos 338-339, 174–188.

Wang, X., Wei, S., Wang, Y., Maung Maung, P., Hubbard, J., Banerjee, P., Huang, B.-S., Moe Oo, K., Bodin, T., Foster, A., Almeida, R., 2019b. A 3-D shear wave velocity model for Myanmar Region. J. Geophys. Res. Solid Earth 124, 504–526.

Weis, D., Kieffer, B., Maerschalk, C., Barling, J., de Jong, J., Williams, G.A., Hanano, D., Pretorius, W., Mattielli, N., Scoates, J.S., Goolaerts, A., Friedman, R.M., Mahoney, J. B., 2006. High-precision isotopic characterization of USGS reference materials by TIMS and MC-ICP-MS. Geochem. Geophys. Geosyst. 7.

Westerweel, J., Roperch, P., Licht, A., Dupont-Nivet, G., Win, Z., Poblete, F., Ruffet, G., Swe, H.H., Thi, M.K., Aung, D.W., 2019. Burma Terrane part of the Trans-Tethyan arc during collision with India according to palaeomagnetic data. Nat. Geosci. 12, 863–868.

Wiedenbeck, M., Allé, P., Corfu, F., Griffin, W.L., Meier, M., Oberli, F., Quadt, A.V., Roddick, J.C., Spiegel, W., 1995. Three natural zircon standards for U-Th-Pb, Lu-Hf, trace element and REE analyses. Geostand. Geoanal. Res. 19, 1–23.

Winchester, J.A., Floyd, P.A., 1977. Geochemical discrimination of different magma series and their differentiation products using immobile elements. Chem. Geol. 20, 325–343.

Winther, T.K., Newton, R.C., 1991. Experimental melting of an hydrous low-K tholeiite: evidence on the origin of Archaean cratons. Bull. Geol. Soc. Den. 39, 213–228.

Woodhead, J.D., Hergt, J.M., 2010. A preliminary appraisal of seven natural zircon reference materials for *in situ* Hf isotope determination. Geostand. Geoanal. Res. 29, 183–195.

Woodhead, J.D., Hergt, J.M., Davidson, J.P., Eggins, S.M., 2001. Hafnium isotope evidence for 'conservative' element mobility during subduction zone processes. Earth Planet. Sci. Lett. 192, 331–346.

Wu, F.-Y., Ji, W.-Q., Liu, C.-Z., Chung, S.-L., 2010. Detrital zircon U–Pb and Hf isotopic data from the Xigaze fore-arc basin: Constraints on Transhimalayan magmatic evolution in southern Tibet. Chem. Geol. 271, 13–25.

Xu, J.-F., Castillo, P.R., 2004. Geochemical and Nd–Pb isotopic characteristics of the Tethyan asthenosphere: implications for the origin of the Indian Ocean mantle domain. Tectonophysics 393, 9–27.

Xu, Y., Liu, C.-Z., Chen, Y., Guo, S., Wang, J.-G., Sein, K., 2017. Petrogenesis and tectonic implications of gabbro and plagiogranite intrusions in mantle peridotites of the Myitkyina ophiolite, Myanmar. Lithos 284-285, 180–193.

Yao, W., Ding, L., Cai, F.-L., Wang, H.-Q., Xu, Q., Zaw, T., 2017. Origin and tectonic evolution of upper Triassic Turbidites in the Indo-Burman ranges, West Myanmar. Tectonophysics 721, 90–105.

Yin, A., Harrison, T.M., 2000. Geologic evolution of the Himalayan-Tibetan orogen. Annu. Rev. Earth Planet. Sci. 28, 211–280.

Yui, T.-F., Fukoyama, M., Iizuka, Y., Wu, C.-M., Wu, T.-W., Liou, J.G., Grove, M., 2013. Is Myanmar jadeitite of Jurassic age? A result from incompletely recrystallized inherited zircon. Lithos 160-161, 268–282.

Zaw, Khin, 1990. Geological, petrogical and geochemical characteristics of granitoid rocks in Burma: with special reference to the associated W Sn mineralization and their tectonic setting. J. SE Asian Earth Sci. 4, 293–335.

Zeng, L., Gao, L.E., Xie, K., Jing, L.Z., 2011. Mid-Eocene high Sr/Y granites in the Northern Himalayan Gneiss Domes: Melting thickened lower continental crust. Earth Planet. Sci. Lett. 303, 251–266.

Zhang, S.Q., Mahoney, J.J., Mo, X.X., Ghazi, A.M., Milani, L., Crawford, A.J., Guo, T.Y., Zhao, Z.D., 2005. Evidence for a widespread tethyan upper mantle with Indian-Ocean-Type isotopic characteristics. J. Petrol. 46, 829–858.

Zhang, P., Mei, L., Hu, X., Li, R., Wu, L., Zhou, Z., Qiu, H., 2017. Structures, uplift, and magmatism of the Western Myanmar Arc: Constraints to mid-Cretaceous-Paleogene tectonic evolution of the western Myanmar continental margin. Gondwana Res. 52, 18–38.

Zhang, J.E., Xiao, W., Windley, B.F., Wakabayashi, J., Cai, F., Sein, K., Wu, H., Naing, S., 2018. Multiple alternating forearc- and backarc-ward migration of magmatism in the Indo-Myanmar Orogenic Belt since the Jurassic: Documentation of the orogenic architecture of eastern Neotethys in SE Asia. Earth Sci. Rev. 185, 704–731.

Zhang, X., Chung, S.-L., Lai, Y.-M., Ghani, A.A., Murtadha, S., Lee, H.-Y., Hsu, C.-C., 2019. A 6000-km-long Neo-Tethyan arc system with coherent magmatic flare-ups and lulls in South Asia. Geology 47, 573–576.

Zhang, G., He, Y., Ai, Y., Jiang, M., Mon, C.T., Hou, G., Thant, M., Sein, K., 2021a. Indian continental lithosphere and related volcanism beneath Myanmar: Constraints from local earthquake tomography. Earth Planet. Sci. Lett. 567, 116987.

Zhang, L., Fan, W., Ding, L., Pullen, A., Ducea, M.N., Li, J., Wang, C., Xu, X., Sein, K., 2021b. Forced subduction initiation within the Neotethys: an example from the mid-cretaceous Wuntho-Popa arc in Myanmar. GSA Bull. https://doi.org/10.1130/B35818.1.

Zhang, Y.-Z., Wang, X.-L., Li, J.-Y., He, Z.-Y., Zhang, F.-F., Chen, X., Wang, S., Du, D.-H., Huang, Y., Jiang, C.-H., 2021c. Oligocene leucogranites of the Gangdese Batholith, Southern Tibet: fractional crystallization of felsic melts from Juvenile lower crust. J. Petrol. 62 https://doi.org/10.1093/petrology/egab076.

Zhu, D.-C., Chung, S.-L., Mo, X.-X., Zhao, Z.-D., Niu, Y., Song, B., Yang, Y.-H., 2009. The 132 Ma Comei-Bunbury large igneous province: Remnants identified in present-day southeastern Tibet and southwestern Australia. Geology 37, 583–586.